



The 2011 Tohoku Tsunami on the Coast of Mexico: A Case Study

OLEG ZAYTSEV,¹ ALEXANDER B. RABINOVICH,^{2,3} and RICHARD E. THOMSON²

Abstract—The Tohoku (East Japan) earthquake of 11 March 2011 (M_w 9.0) generated a great trans-oceanic tsunami that spread throughout the Pacific Ocean, where it was measured by numerous coastal tide gauges and open-ocean DART (Deep-ocean Assessment and Reporting of Tsunamis) stations. Statistical and spectral analyses of the tsunami waves recorded along the Pacific coast of Mexico have enabled us to estimate the principal parameters of the waves along the coast and to compare statistical features of the tsunami with other tsunamis recorded on this coast. We identify coastal “hot spots”—Manzanillo, Zihuatanejo, Acapulco, and Ensenada—corresponding to sites having highest tsunami hazard potential, where wave heights during the 2011 event exceeded 1.5–2 m and tsunami-induced currents were strong enough to close port operations. Based on a joint spectral analysis of the tsunamis and background noise, we reconstructed the spectra of tsunami waves in the deep ocean and found that, with the exception of the high-frequency spectral band (>5 cph), the spectra are in close agreement with the “true” tsunami spectra determined from DART bottom pressure records. The departure of the high-frequency spectra in the coastal region from the deep-sea spectra is shown to be related to background infragravity waves generated in the coastal zone. The total energy and frequency content of the Tohoku tsunami is compared with the corresponding results for the 2010 Chilean tsunami. Our findings show that the integral open-ocean tsunami energy, I_0 , was ~ 2.30 cm², or approximately 1.7 times larger than for the 2010 event. Comparison of this parameter with the mean coastal tsunami variance (451 cm²) indicates that tsunami waves propagating onshore from the open ocean amplified by 14 times; the same was observed for the 2010 tsunami. The “tsunami colour” (frequency content) for the 2011 Tohoku tsunami was “red”, with about 65% of the total energy associated with low-frequency waves at frequencies <1.7 cph (periods >35 min). The “red colour” (i.e., the prevalence of low-frequency waves) in the 2011 Tohoku, as well as in the 2010 Chile tsunamis, is explained by the large extension of the source areas. In contrast, the 2014 and 2015 Chilean earthquakes had much smaller source areas and, consequently, induced “bluish” (high-frequency) tsunamis.

Key words: 2011 Tohoku tsunami, Mexican coast, tide gauge records, DART, open-ocean measurements, tsunami travel time, spectral analysis.

1. Introduction

At 05:46 UTC on 11 March 2011, a great thrust-fault earthquake of magnitude M_w 9.0 occurred off the coast of the Tohoku District, north-eastern Honshu Island, Japan. The earthquake, which was the strongest in Japanese history and one of the strongest ever instrumentally recorded in the World Ocean (Simons et al. 2011; Saito et al. 2011), generated a highly destructive tsunami, with run-up heights up to 41 m along the coast of Japan (cf. Mori et al. 2011). The Tohoku (East Japan) tsunami killed nearly 20,000 people and injured thousands of others (Satake et al. 2013). The tsunami also caused major damage to the Fukushima Dai-ichi nuclear power station, creating an ecological catastrophe in the nearby region and giving rise to the discharge of radionuclide ¹³⁷Cs and ¹³⁴Cs into the North Pacific Ocean (Aoyama et al. 2016a, b; Buesseler et al. 2017). The total direct cost of damage associated with the tsunami in Japan is about 300 billion dollars.

The 2011 tsunami spread throughout the Pacific Ocean (Fig. 1) and was recorded at numerous off-shore bottom pressure stations and by approximately 250 coastal tide gauges, including those in distant regions, such as French Polynesia (Reymond et al. 2013), New Zealand (Borrero et al. 2013), and Australia (Hinwood and McLean 2013). The tsunami waves strongly affected the West Coast of the USA (Wilson et al. 2013; Borrero and Greer 2013; Xing et al. 2013; Admire et al. 2014) and the west coast of British Columbia, including sheltered straits, inlets,

¹ Instituto Politécnico Nacional, Centro Interdisciplinario de Ciencias Marinas, Ave. IPN, s/n, Playa Palo de Santa Rita, 23096 La Paz, BCS, Mexico.

² Department of Fisheries and Oceans, Institute of Ocean Sciences, 9860 West Saanich Road, Sidney, BC V8L 4B2, Canada. E-mail: A.B.Rabinovich@gmail.com

³ Russian Academy of Sciences, P.P. Shirshov Institute of Oceanology, 36 Nakhimovskiy Prosp, Moscow 117997, Russia.

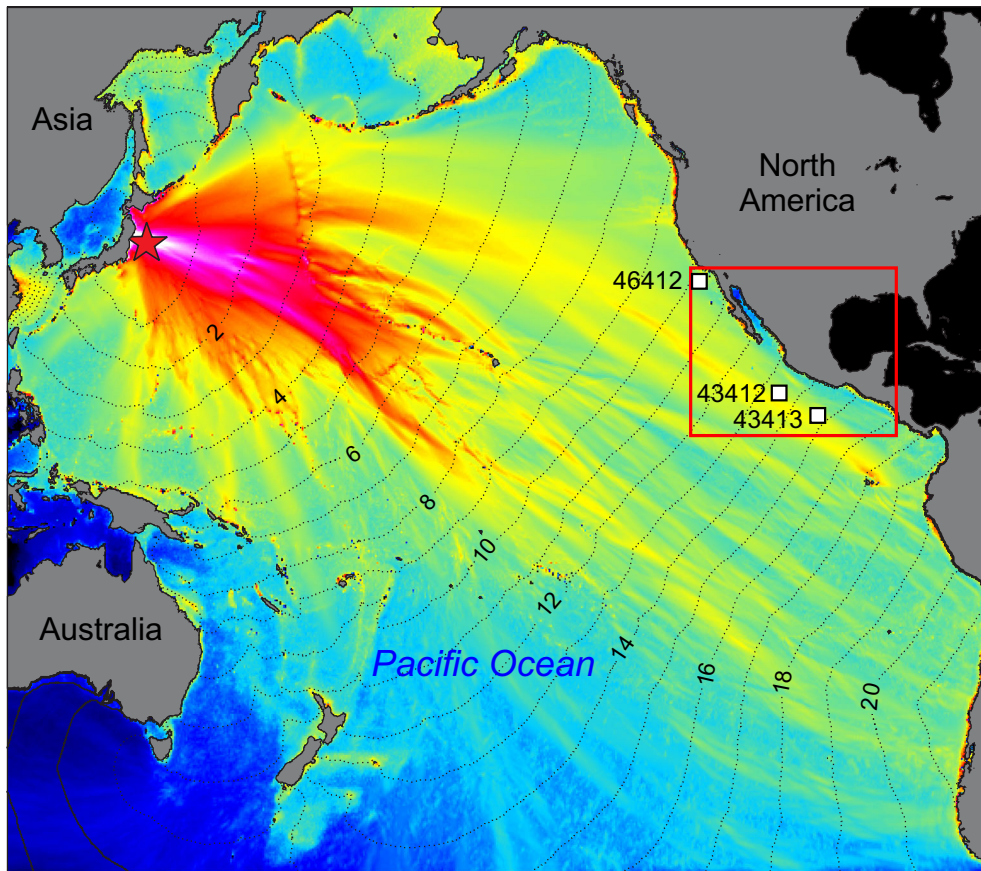


Figure 1

Numerically simulated maximum tsunami amplitudes for the 2011 Tohoku (East Japan) tsunami in the Pacific Ocean (modified from Fine et al. 2013). The earthquake epicenter is indicated by the *red star*. The DART stations off the Mexican coast are denoted by *white squares*. *Black dotted lines* show the 2011 tsunami travel time (in hours) from the source area. The *red box* indicates the study region

and harbours (cf. Thomson et al. 2013). The recorded tsunami data were used by Tang et al. (2012), Wei et al. (2013), Fine et al. (2013), and Rabinovich et al. (2013a) to examine tsunami energy propagation, transformation, and decay in the Pacific Ocean, and by Song et al. (2012), Saito et al. (2011), and Heidarzadeh and Satake (2013) to reconstruct characteristics of the tsunami source region.

The 2011 Tohoku tsunami was recorded extensively on the Pacific coast of Mexico and was the highest tsunami observed on this coast since the 1960 Chile and 1964 Alaska tsunamis. It was also the first recorded tsunami from a source area located near Japan since the moderate event of 16 May 1968 [see Sanchez and Farreras (1993) for a description of historical tsunamis on the Mexican coast]. Although

we could find no official reports on damage associated with the 2011 tsunami along the coast of Mexico, it appears that currents induced in some ports and harbours were significant and dangerous, similar to those recorded in southern California (Wilson et al. 2013; Admire et al. 2014).

Recently, we (Zaytsev et al. 2016) examined three Chilean tsunamis (2010, 2014, and 2015) observed along the coast of Mexico in order to estimate and compare the main physical properties of these events and to identify coastal “hot spots”, i.e., sites with significantly amplified tsunami wave heights. Based on joint spectral analyses of the coastal tsunami records and background oscillations, we were also able to reconstruct the open-ocean spectra for the three Chilean tsunamis and found them to be in close

agreement with the actual tsunami spectra determined from direct analysis of the DART¹ records observed offshore of Mexico. We introduced major tsunami parameters describing individual events: specifically, the integral open-ocean energy (I_0), the mean amplification factor (A) of tsunami waves approaching the coast from the open-ocean, and the frequency composition (“tsunami colour”). The open-ocean and coastal tsunami spectra were then used to calculate these parameters and intercompare them for the three events.

The 2011 Tohoku tsunami originated on the opposite side of the Pacific Ocean compared to the 2010, 2014, and 2015 Chilean tsunamis. While the Chilean tsunamis reached the Mexican coast by propagating along the coasts of South and Central America, the Tohoku tsunami reached the coast after crossing the Pacific Ocean. The questions of high importance are: How different are the open-ocean parameters of tsunami waves arriving at the coast of Mexico from so markedly different sources? Are the coastal responses and locations of “hot spots” of high risk identified along the Mexican coast for the Chilean tsunamis the same as those for the Tohoku tsunami?

The 2011 Tohoku tsunami was the strongest tsunami ever digitally recorded on the Mexican coast. The high-quality data obtained from onshore and offshore instruments for this event were crucial for determining the general properties of tsunami waves in this region. In addition, the data are shown to be valuable for comparing the Tohoku tsunami with the Chilean tsunamis to improve the tsunami warning service and to mitigate the threat of possible future Pacific Ocean tsunamis for coastal areas of Mexico.

2. Observations

The 2011 Tohoku tsunami was measured on the Pacific coast of Mexico by a number of high-quality

digital coastal tide gauges and offshore by NOAA DART bottom pressure recorders, BPRs (Fig. 2). The tide gauge network on the Pacific coast of Mexico consists of two major components: (1) *The National Mareographic Service*, operated by the Institute of Geophysics, National Autonomous University of Mexico (UNAM) (<http://www.mareografico.unam.mx>); and (2) the north-western net of sea-level monitoring operated by *The Laboratory of Sea Level*, Center for Scientific Research and Graduate Studies of Ensenada, Baja California, Mexico (CICESE, <http://www.redmar.cicese.mx>). All tide gauges operated by (1) have a radar sensor and satellite data transmission system; some gauges have an additional pressure sensor. The sampling interval in 2011 was 1 min at Puerto Vallarta, Zihuatanejo, Acapulco, and Huatulco and 6 min at Mazatlan, Lazaro Cardenas, Salina Cruz, and Puerto Madero (Puerto Chiapas). All sea-level data from the 6 tide gauges operated by (2) are stored at 1-min intervals.

Two types of offshore DART data have been used in our examination of the 2011 Tohoku tsunami (see Mungov et al. 2013; Rabinovich and Eblé 2015 for a description of the DART data): (1) “Event-mode” data, which are transmitted after the start of the event in real-time for several hours at pre-defined 1-min intervals; and (2) 15-s tsunami data, which are stored in the instrument and then downloaded following retrieval of the DART BPR. The event-mode data were used to estimate a select suite of statistical tsunami wave parameters in the open ocean (in particular, arrival times and maximum wave heights of the incoming tsunami waves), which are compared with similar parameters from other DART and coastal sites. The 15-s data were used for more extensive analyses of open-ocean tsunami properties, including spectral analysis and evaluation of the tsunami energy. There were three DARTs operating near the coast of Mexico in 2011 (Fig. 2): for two of them (46412 and 43413), long series of downloaded 15-s data are available, while for DART 43412, we have only the “event-mode” series. The data from these three DARTs were also used by Rabinovich et al. (2013a) to examine the open-ocean energy decay and by Eblé et al. (2015) to investigate the leading negative phase of the propagating tsunami waves. The DART data were obtained from the National Centers

¹ DART = Deep-ocean Assessment and Reporting of Tsunamis, is an effective network of deep-ocean stations elaborated for continuous monitoring of tsunami waves in the open ocean and early tsunami warning (cf. Titov 2009; Mofjeld 2009; Mungov et al. 2013; Rabinovich and Eblé 2015).

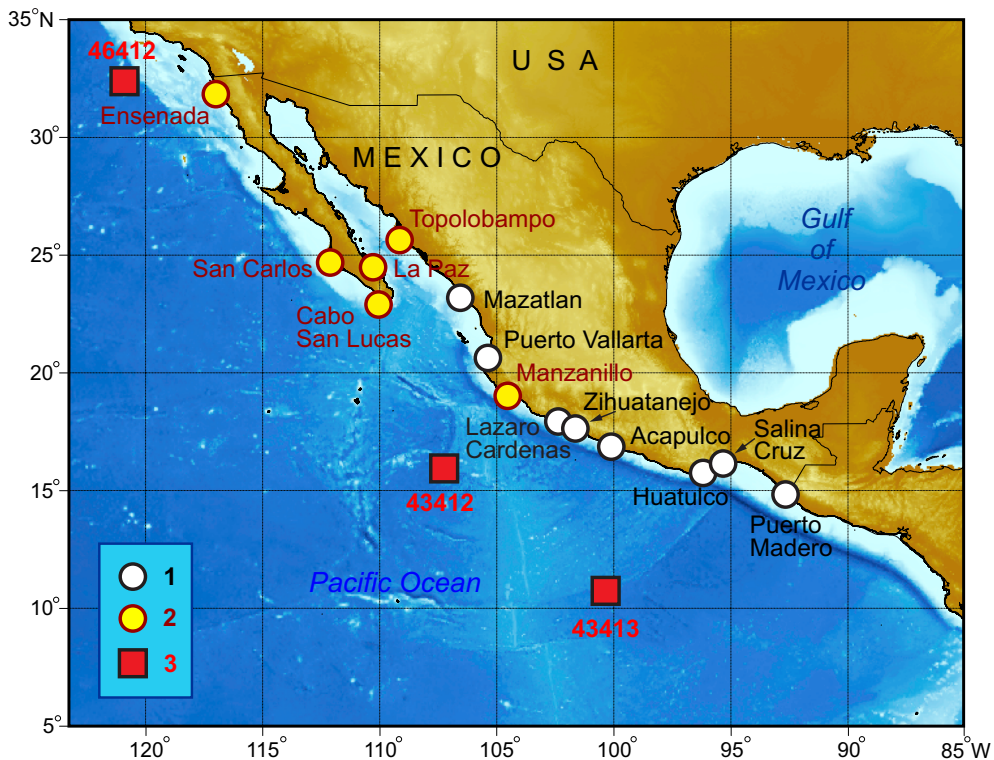


Figure 2

Map of coastal Mexico showing the location of the tide gauges operated by: (1) UNAM and (2) CICESE; (3) denotes the three open-ocean DART stations located near the coast of Mexico

for Environmental Information (NCEI), NOAA, Boulder, Colorado, and the National Data Buoy Center (NDBC), NOAA, Stennis Space Center, Mississippi.

Coastal and open-ocean data with the same sampling intervals as those discussed above were used by Zaytsev et al. (2016) to examine the 2010, 2014, and 2015 Chilean tsunamis; some additional details on the data may be founded in that paper. Here, Table 1 summarizes the coastal and offshore data available for the 2011 event for the Mexican sites. The digital records from all coastal and open-ocean stations have been examined using the data analysis procedures and tsunami detection methods described by Rabinovich et al. (2006, 2013b) and Zaytsev et al. (2016). We checked all data, verified them, corrected any errors, filled gaps, and removed spikes. The tides were calculated using the least-squares method (cf. Parker 2007) and subtracted from the original records; the resulting residual time series were used in all subsequent analyses. To suppress low-frequency sea-level

fluctuations, mainly associated with atmospheric processes, and to simplify tsunami detection, we high-pass filtered the de-tided time series using a 4-h Kaiser–Bessel (KB) window (cf. Thomson and Emery 2014). These filtered series were then used to construct plots of tsunami records for various sites and to estimate certain statistical characteristics of the waves. To examine the spectral properties of the tsunami oscillations, we used the unfiltered residual time series.

3. Data Analyses

There were 14 coastal tide gauges in operation on the Pacific coast of Mexico at the time of the 2011 Tohoku tsunami (Fig. 3a, b): ten with 1-min sampling and four with 6-min sampling. These coastal records were complemented by data from three offshore DARTs (Table 1).

Table 1

Tide gauges and DART stations that recorded the 2011 Tohoku tsunami on the Pacific coast and offshore of Mexico

No.	Station	Data source	Coordinates		Sampling interval (min)
			Latitude°N	Longitude°W	
1	Ensenada	CICESE	31°50.9'	116°37.1'	1
2	Topolobampo	CICESE	25°21.0'	109°02.0'	1
3	San Carlos	CICESE	24°28.3'	112°04.3'	1
4	La Paz	UNAM	24°16.0'	110°20.0'	1
5	Cabo San Lucas	CICESE	22°31.7'	109°32.7'	1
6	Mazatlan	UNAM	23°10.9'	106°25.4'	6
7	Puerto Vallarta	UNAM	20°39.5'	105°14.6'	1
8	Manzanillo	CICESE	19°03.8'	104°17.9'	1
9	Lazaro Cardenas	UNAM	17°56.4'	102°10.7'	6
10	Zihuatanejo	UNAM	17°38.2'	101°33.5'	1
11	Acapulco	UNAM	16°50.3'	99°54.2'	1
12	Huatulco	UNAM	15°45.2'	96°7.8'	1
13	Salina Cruz	UNAM	16°19.1'	95°11.8'	6
14	Puerto Madero	UNAM	14°42.7'	92°24.1'	6
15	DART 46412 (3770 m)	NCEI/NDBC	32°27.9'	120°34.5'	0.25
16	DART 43412 (3065 m)	NDBC	16°01.6'	106°59.8'	1 ^a
17	DART 43413 (3560 m)	NCEI/NDBC	10°50.5'	100°08.2'	0.25

The water depth for each DART station appears in the brackets

^a “Event-mode” DART data

UNAM Institute of Geophysics, National Autonomous University of Mexico, CICESE Center for Scientific Research and Graduate Studies of Ensenada, Baja California, Mexico, NTCW National Tsunami Warning Center, Palmer, Alaska, USA, NCEI National Centers for Environmental Information, NOAA, Boulder, Colorado, USA, NDBC National Data Buoy Center, NOAA, Stennis Space Center, Mississippi, USA

3.1. Statistical Analysis

We have used the tsunami records from the various sites to estimate statistical parameters of the tsunami waves, including wave arrival times, maximum wave heights, and wave periods (Table 2). Observed travel times of the arriving waves were also compared with the travel times (Fig. 1) computed by the “wave-front orientation method” (Fine and Thomson 2013). The analyses yielded several important features of the 2011 Tohoku tsunami waves on the coast of Mexico (Table 2; Figs. 3a, b, 4):

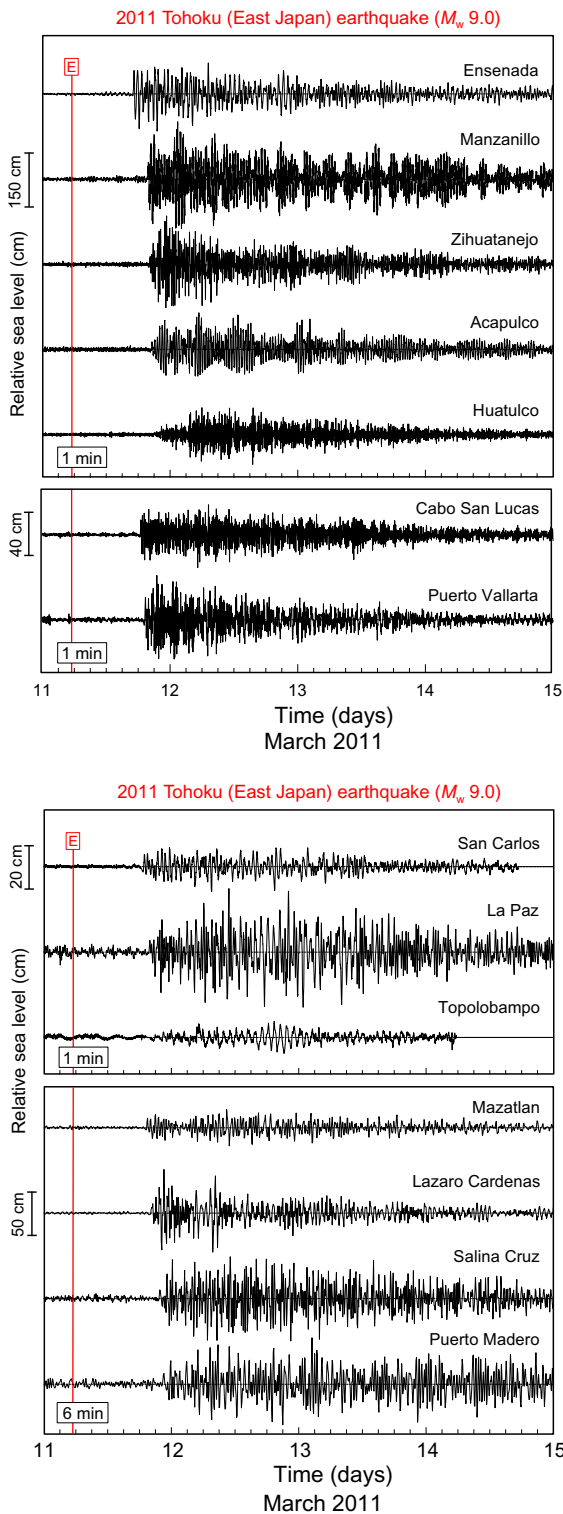
1. The 2011 Tohoku tsunami was clearly recorded along the entire Pacific coast of Mexico. The highest trough-to-crest wave heights were observed at Manzanillo (258 cm), Zihuatanejo (258 cm), Ensenada (190 cm), and Acapulco (187 cm). At Lazaro Cardenas, located between Acapulco and Manzanillo, the maximum wave height was only 95 cm (Fig. 4). The Lazaro Cardenas station also recorded relatively small tsunami signals during the 2010, 2014, and 2015 Chilean tsunamis (Zaytsev et al. 2016). In general, the observed tsunami wave heights for the

2011 Tohoku event were 20–30% greater than for the 2010 Chile event, except Acapulco where this ratio was 1.9.

2. The smallest wave heights were at Topolobampo (13 cm) and San Carlos (20 cm); the quality of the records at these tide gauges was sufficient to estimate the main statistical characteristics of the tsunami waves, but not sufficient for further spectral analysis.

3. Along the Mexican coast, the 2011 Tohoku tsunami waves were first recorded on 11 March 2011 at 16:58 UTC at Ensenada, the northernmost Mexican tide gauge station, and then recorded progressively southward at other stations. Finally, at 22:18 UTC, the tsunami arrived at Puerto Madero, the southernmost Mexican station. The respective travel times of 11 h 12 min (Ensenada) and 16 h 32 min (Puerto Madero) after the main shock are in good agreement with the numerically estimated tsunami travel times (Fig. 4).

5. The observed wave periods in the first hours after the arrival of tsunami waves can be separated



◀Figure 3

The 11 March 2011 Tohoku tsunami recorded by tide gauges at 14 sites on the coast of Mexico. Time series are the residual sea levels obtained by removing the calculated tides from the original time series and then high-pass filtering the resulting de-tided time series with a 4-h Kaiser-Bessel window. The *solid vertical red line* labelled “E” denotes the time of the earthquake. The sampling interval of the corresponding records is indicated

into three groups: (1) 17–21 min at Ensenada, La Paz, Puerto Vallarta, Manzanillo, Lazaro Cardenas, and Zihuatanejo; (2) 28–31 min at San Carlos, Mazatlan, Acapulco, Salina Cruz, and Puerto Madero; and (3) 11–13 min at Cabo San Lucas and Huatulco.

6. Maximum wave amplitudes at most sites were observed hours after the first-wave arrival, ranging from 2 h at Puerto Vallarta to 21 h at Topolobampo.

7. The signal-to-noise (s/n) ratio was high at all stations, making it possible to define the first-wave arrival time very precisely. The leading wave at all sites was positive (a “crest wave”).

8. The tsunami ringing at all stations was long, lasting for 4–5 days. The ringing time is comparable to that observed on the Mexican coast after the 2010, 2014, and 2015 Chilean tsunamis (Zaytsev et al. 2016) and in good agreement with open-ocean observations of the 2011 tsunami (Rabinovich et al. 2013a).

It is known that the sampling interval affects measured tsunami wave heights and other characteristics of tsunami waves. This effect can be considerable, especially for high-frequency events (Candella et al. 2008). However, even low-frequency observed tsunami heights are attenuated when recorded at long sampling intervals. For example, the maximum 2004 Sumatra tsunami height at Manzanillo (Mexico) recorded at 2-min sampling was 12 cm (14%) higher than the height originally estimated from a 6-min record (Rabinovich et al. 2006, 2011). Zaytsev et al. (2016) found that during the 2010 Chile tsunami at Acapulco, the wave heights recorded by the UNAM (6-min) gauge were approximately 30% smaller than those recorded by the CICESE (1-min) gauge. Candella et al. (2008) estimated that the mean attenuation coefficient, R ,

Table 2

Parameters of the Tohoku tsunami of 11 March 2011 recorded on the coast of Mexico

Station	Sampling (min)	First wave			Maximum waves			Observed tsunami variance (cm ²)	Visually estimated periods (min)
		Arrival time (UTC)	Travel time (hh:mm)	Amp. (cm) Sign	Amp. (cm)	Time (UTC) of peak amplitude	Wave height (cm)		
1. Ensenada	1	16:58	11:12	+68.0	88.0	7:09 ^a	190	749	17, 42
2. San Carlos	1	18:44	12:58	+7.2	11.0	8:32 ^a	20	12	29, 47
3. C. San Lucas	1	18:20	12:34	+14.0	23.0	7:12 ^a	56	71	13
4. La Paz	1	19:45	13:59	+5.8	29.2	10:49 ^a	52	73	21, 31
5. Topolobampo	1	22:18	16:32	+3.5	8.7	19:19 ^a	13	7	–
6. Mazatlan	6	19:18	13:32	+9.0	17.0	10:30 ^a	43	52	31
7. P. Vallarta	1	19:17	13:31	+14.7	34.0	21:30	78	95	18
8. Manzanillo	1	19:34	13:48	+43.0	127.0	1:24 ^a	258	1627	19, 35
9. L. Cardenas	6	20:03	14:17	+7.2	44.0	22:30	95	131	19, 46
10. Zihuatanejo	1	20:05	14:19	+24.0	137.0	23:14	258	930	18, 35
11. Acapulco	1	20:22	14:37	+23.0	107.0	5:14 ^a	187	852	29
12. Huatulco	1	21:14	15:28	+7.1	65.0	5:54 ^a	126	276	11
13. Salina Cruz	6	21:36	15:50	+11.0	42.0	11:00 ^a	87	284	28
14. P. Madero	6	22:18	16:32	+11.0	48.0	8:42 ^a	86	281	29
DART 46412 ^b	0.25	15:58	10:12	+11.7	11.7	16:08	18	3.21	6, 14
DART 43412	0.25	19:09	13:23	+13.7	13.7	19:12	23	4.17	7, 15
DART 43413	0.25	20:37	14:51	+19.2	19.2	20:49	35	5.21	7, 15

All times are in UTC for 11 March, except where indicated. The main shock of the M_w 9.0 earthquake off Japan was at 05:46 UTC

^a 12 March 2011

^b “Event-mode” data

for wave heights measured at 6-min relative to 1-min is $R \sim 0.8$ for major (low-frequency) events. Thus, we can expect that the evaluated heights for 6-min stations (Mazatlan, Lazaro Cardenas, Salina Cruz, and Puerto Madero; Table 2) are underestimated by 20–30% and the actual maximum tsunami wave heights at these stations, except Mazatlan, were more than 1 m.

The mean tsunami wave height for the 2011 Tohoku event on the Mexican coast, averaged over 12 records (excluding San Carlos and Topolobampo), is 126.1 cm, which is 1.3 times greater than for the 2010 Chile tsunami. Maximum tsunami variances (estimated for 34-h tsunami segments) are: Manzanillo (1627 cm²), Zihuatanejo (930 cm²), Acapulco (852 cm²), and Ensenada (749 cm²); the mean variance (Var_0) averaged over all records is 451 cm². Our estimates of maximum wave heights and tsunami variance clearly pinpoint local “hot spots” (Manzanillo, Zihuatanejo, Acapulco and Ensenada), where tsunami waves were considerably higher than the mean (Fig. 5).

To examine the properties of the 2011 tsunami waves seaward of the Mexican coast, we used three open ocean DART stations (Fig. 2, Table 1). For two DARTs, 46412 and 43413, we took advantage of long, high-quality 15-s data downloaded from the retrieved instruments; for DART 43412, we used several hours of 1-min “event-mode” data (see Mungov et al. 2013 and Rabinovich and Eblé 2015 for details of the DART operations). The DART records of the 2011 Tohoku tsunami waves (Fig. 4) differ markedly from the coastal tsunami records. The coastal records have different individual characteristics (Fig. 3a, b), whereas the open-ocean records from DARTs located 3000 km from each other look similar (the open-ocean tsunami signal was spatially uniform).

A noteworthy characteristic of the DART 46412, 43412, and 43413 records was the presence of a small (2–3 cm), but distinctive, sea-level subsidence (“trough”) preceding the leading frontal crest wave (Fig. 4b). A similar feature was observed by the same DARTs for the 2010 Chile tsunami (Zaytsev et al.

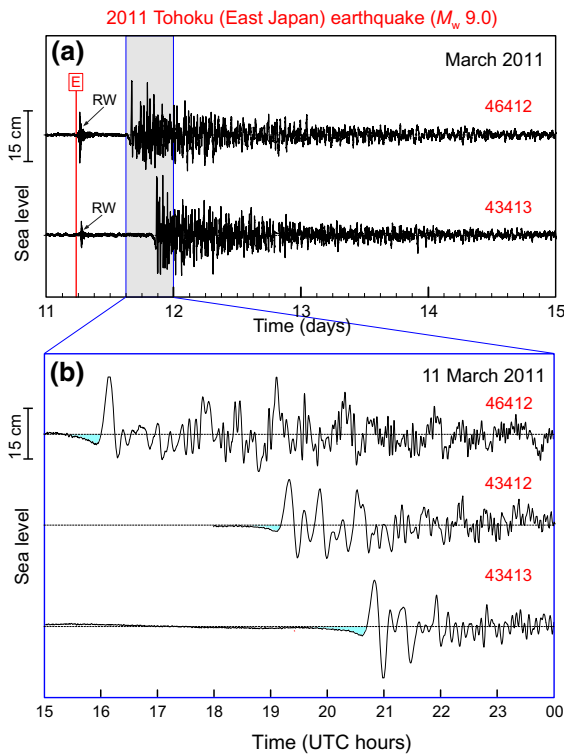


Figure 4

a Three-day records of the 2011 Tohoku tsunami downloaded as 15-s data from DARTs 46412 and 43413 off the coast of Mexico; and **b** 9-h zoomed records from the DARTs in (a) and from the 1-min “event-mode” record for DART 43412. The records have been de-tided but not high-pass filtered. The *light blue shaded areas* are the “negative phase” of the open-ocean tsunami records associated with subsidence of Earth’s crust under the tsunami wave loading (cf. Watada et al. 2014; Eblé et al. 2015)

2016) and in most of the other 2010 and 2011 DART records throughout the Pacific Ocean (Eblé et al. 2015). According to Watada et al. (2014), the “trough” was the result of the elastic response of the solid earth (crustal mass deformation) during tsunami propagation and to the additional effects of seawater compressibility and gravitational potential changes. Consequently, the leading tsunami wave at all three near-Mexico DART stations was actually positive, with maximum observed amplitudes of 12–19 cm (Table 2) corresponding to the first wave. The open-ocean records of the 2010 Chilean tsunami at these DART sites had similar features with maximum amplitudes (8–14 cm) for the first wave (Zaytsev et al. 2016).

The observed wave arrival times at the DARTs are consistent with the arrival times from the coastal

measurements and with the theoretically computed travel times shown in Fig. 5. These times are only a little longer than the Estimated Times of Arrival (ETA) evaluated by the National Tsunami Warning Center (NTWC, Palmer, AK): 15:45 UTC (46412), 18:50 (43412), and 20:15 (43413). The differences (see Table 2) range from 13 to 22 min, or roughly 2–2.5% of the travel times. For comparison, these differences were from 5 to 13 min (1–1.7%) for the 2010 Chilean tsunami. We note that the NTWC ETA estimates are in better agreement with the observed arrival times for coastal stations than for DARTs: the ETAs are 18:19 UTC (Cabo San Lucas), 19:32 (Manzanillo), and 20:20 (Acapulco), corresponding to differences from our estimates (Table 2) of only 1–2 min.

The travel time estimates from DART/coastal measurements (Table 2) and from numerical computations (Fig. 5) show that the tsunami waves propagated in the southeast direction along the continental margin of Mexico; the time difference in arrival times between Ensenada (the northernmost tide gauge station) and Puerto Madero (the southernmost station) was 5 h 20 min.

3.2. Time–Frequency Analysis

To examine temporal variations of the recorded 2011 Tohoku tsunami waves in the frequency domain, we used a multiple-filter method, which is similar to wavelet analysis (cf. Thomson and Emery 2014) and is based on narrow-band filters with a Gaussian window that isolates a specific centric frequency, $\omega_n = 2\pi f_n$. This method, which has been used effectively to examine various tsunami events (cf. Rabinovich et al. 2006, 2013b), enables us to determine changes in tsunami waves as a function of frequency, f , and time, t , and to construct the so-called “ f – t diagrams” that display possible dispersion of the propagating waves.

We selected 3-day data segments (11–14 March 2011) and constructed f – t diagrams for the frequency band of 0.3–30 cph (for 1-min coastal records) and 0.3–5 cph (for 6-min coastal records). The resulting plots are shown in Fig. 6a, b, respectively. For the f – t diagrams of the 15-s DART records, we also used the frequency band of 0.3–30 cph (Fig. 6c). The plots

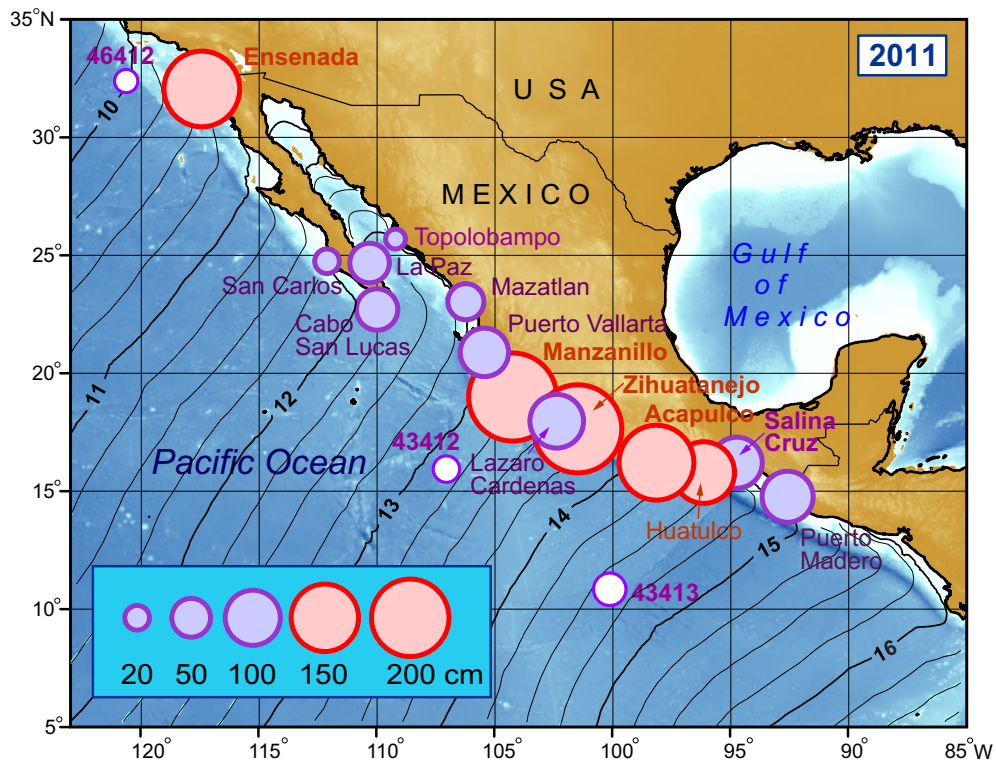


Figure 5

Map of coastal Mexico showing the maximum recorded wave heights at the fourteen tide gauge sites and three offshore DART stations for the 2011 Tohoku tsunami. The size of a circle is proportional to the maximum recorded trough-to-crest wave height: 'pink' denotes heights above the mean value of 126 cm, while 'purple' denotes heights below this value. Black solid lines show the 2011 tsunami travel time (in hours and 15 min) from the source area

reveal very abrupt and distinct appearances of the tsunami waves; the wave arrival times are clearly evident and consistent among the different sites. At most stations, the waves occupy a relatively broad frequency band, from 0.5–0.75 to 5 cph (periods of 80–120 min) superimposed on narrow, well-defined and persistent frequency bands of significantly amplified energy that are likely associated with the eigen-frequencies of a given site. The most prominent resonant “bands” in the f - t diagrams for individual stations approximately correspond to the following periods: 50 and 30 min at Ensenada; 70 and 30 min at La Paz; 11.5 min at Cabo San Lucas; 8 min at Puerto Vallarta; 37 min at Manzanillo; 20 min at Zihuatanejo; 28 min at Acapulco (Fig. 6a); 37 min at Mazatlan; 55 and 18 min at Lazaro Cardenas (Fig. 6b); and 20–30 min at DARTs 46412 and 43413 (Fig. 6c). A specific feature of the f - t diagrams for all coastal records is the long ringing time and

slow energy decay at all tsunami frequencies (Fig. 6a, b). In contrast, the open-ocean (DART) tsunami records reveal much faster decay times (Fig. 6c).

We have not examined the specific effect of dispersion on the observed records, but dispersion is clearly evident in the high-frequency “tails” (frequencies >12 cph, i.e., periods <5 min) of some of the coastal records, in particular those for Ensenada, Puerto Vallarta, Zihuatanejo, Acapulco, and Huatulco (Fig. 6a). Dispersion is also present in the DART records (Fig. 6c).

3.3. Spectral Analysis

The spectra of observed sea-level oscillations during a tsunami event may be represented as a superposition of the “true” tsunami spectrum, $S_{\text{tsu}}(\omega)$, and the background spectrum, $S_{\text{bg}}(\omega)$:

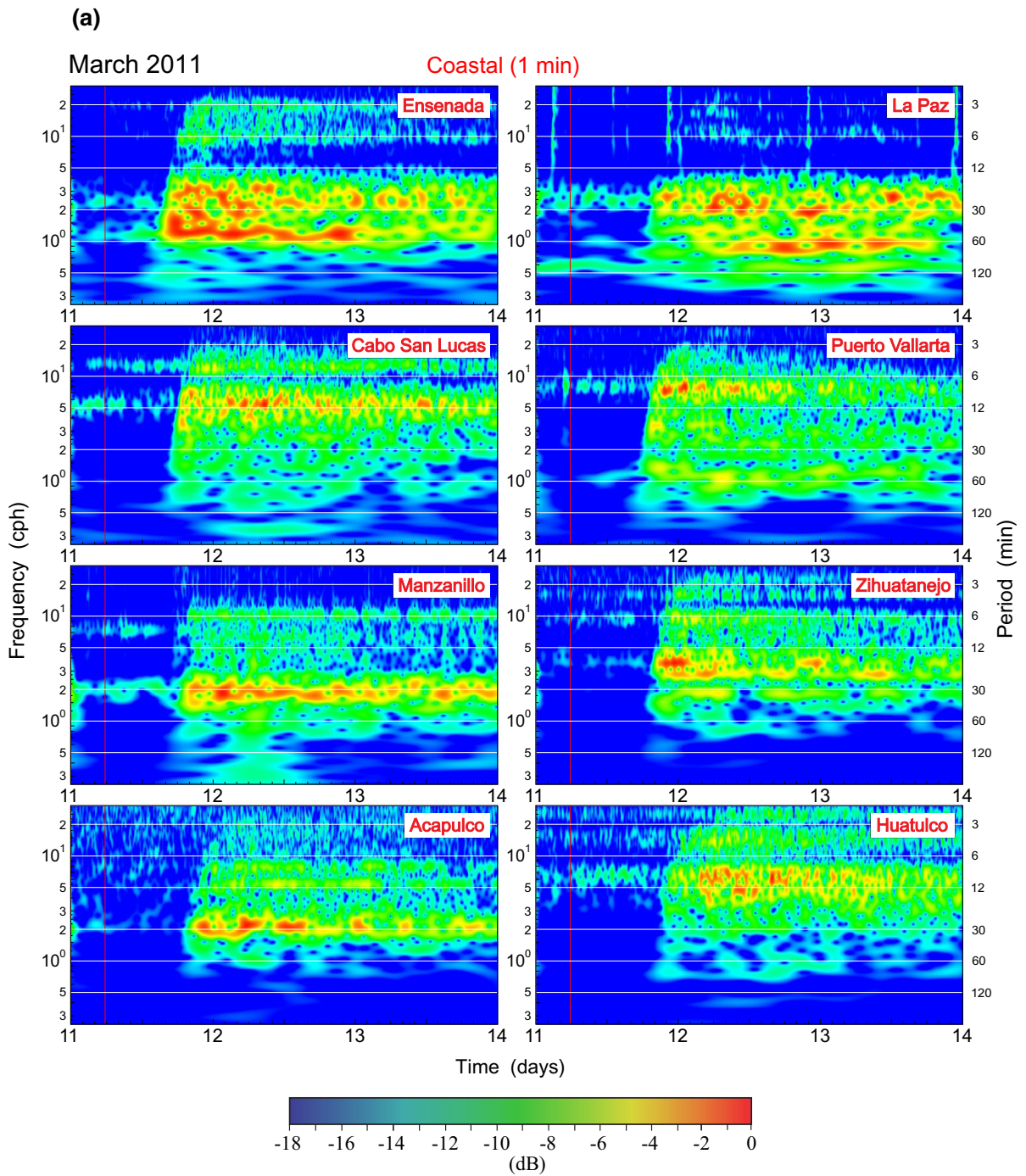


Figure 6

Frequency–time plots (f - t diagrams) for the 11 March 2011 Tohoku tsunami records for: **a** eight coastal 1-min records; **b** four coastal 6-min records; and **c** two open-ocean DART records. The *solid vertical red line* labelled *E* denotes the time of the earthquake

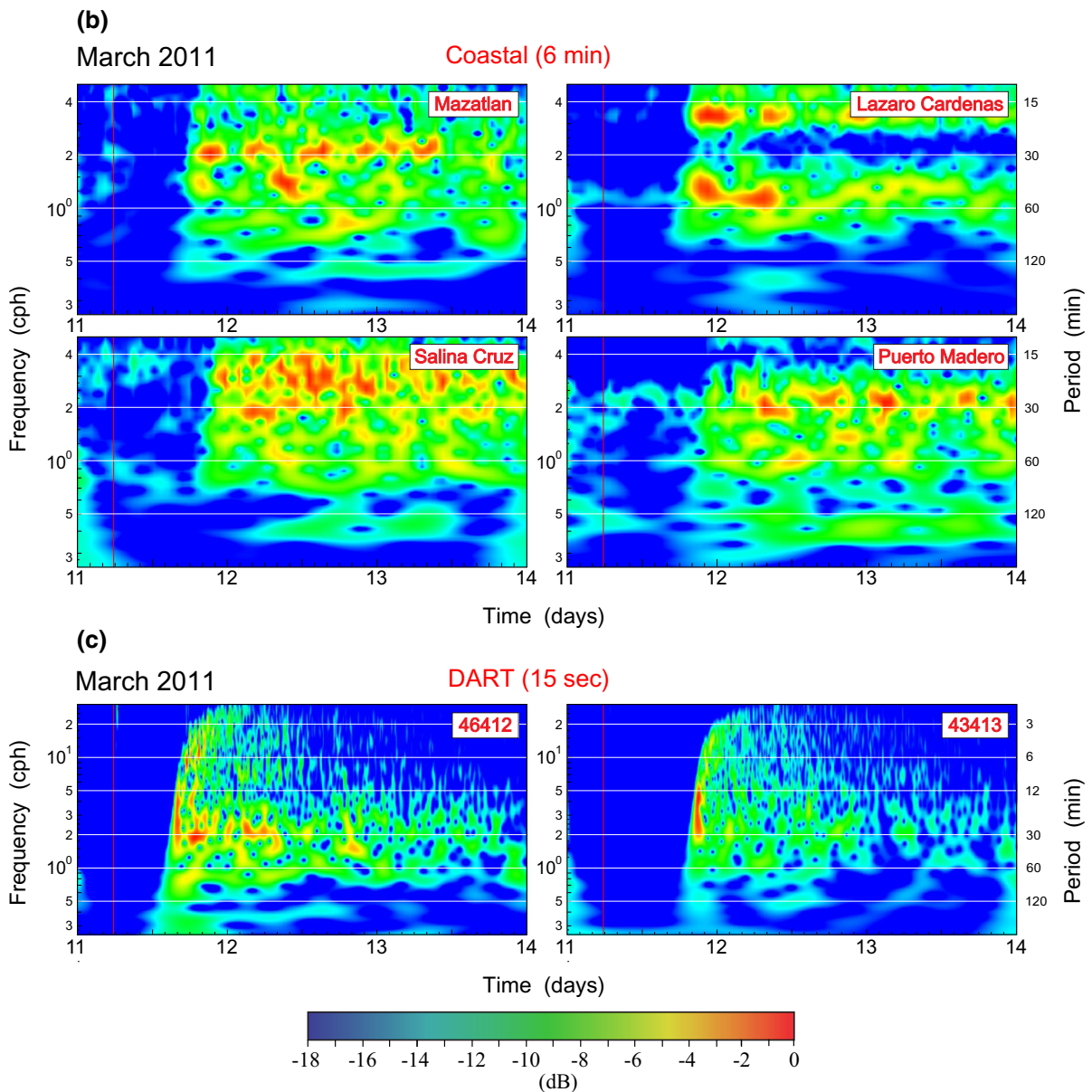


Figure 6 continued

$$S_{\text{obs}}(\omega) = S_{\text{tsu}}(\omega) + S_{\text{bg}}(\omega), \quad (1)$$

where ω is the angular frequency. In practice, the exact background spectrum, $S_{\text{bg}}(\omega)$, during the event is unknown, but we can assume that it is approximately the same as before the event.

To examine the spectral properties of tsunami oscillations during the 11 March 2011 Tohoku tsunami and to compare these properties with those

of the background oscillations at the same sites and with spectra of other events, we separated the records into two parts: (a) the pre-tsunami period (duration of 5.6 days for the four 6-min stations and 4.6 days for the eight 1-min stations), which we used for the background analysis; and (b) the period of 32 h (34 h for 1-min data) following the tsunami wave arrival, which we used for the tsunami analysis. Our spectral analysis procedure is similar to that described by

Thomson and Emery (2014) (see also, Rabinovich et al. 2013b; Zaytsev et al. 2016). To improve the spectral estimates, we used a Kaiser–Bessel (KB) spectral window with half-window overlaps prior to the Fourier transform. The length of the window was $N = 128$ (768 min) for 6-min records and $N = 512$ (512 min) for 1-min records, yielding $\nu = 40$ (50) degrees of freedom for the background spectra and $\nu = 8$ (14) for the tsunami spectra; the spectral resolution was $\Delta f \approx 0.78(0.117)$ cph and the Nyquist frequency $f_n = 5$ (30) cph for 6-min (1-min) records. The computed tsunami and background spectra for twelve coastal sites are shown in Fig. 7.

There is considerable difference in energy between the tsunami and background spectra. The spectral peaks for the tsunami and the background time series both differ from one coastal station to another, showing the importance of local topographic effects. The most prominent spectral peaks were observed at Ensenada (period of 51 min), Cabo San Lucas (11.5 and 5.1 min), Puerto Vallarta (64 and 8 min), Manzanillo (37 min), Zihuatanejo (35, 21 and 8 min), Lazaro Cardenas (55 and 18 min), and Acapulco (27 and 11 min). These peaks are the same for the tsunami and background spectra, indicating the local resonance origins of the tsunami peaks. This result is in good agreement with the well-known fact that tsunami wave periods recorded at the coast depend on the resonant properties of the local/regional topography rather than on the characteristics of the tsunami source. Thus, the periods of oscillations caused by the tsunami and the long-period background waves on the shelf are almost the same for the same sites. However, at some sites, there some tsunami spectral peaks that are absent in the background spectra. In particular, tsunami spectra at La Paz, Zihuatanejo, and Huatulco have peaks with a period of 73 min, which is probably related to characteristics of the source. In addition, the three most southerly stations, Lazaro Cardenas, Salina Cruz, and Puerto Madero have a pronounced low-frequency peak with a period of 153 min (i.e., ~ 2.5 h). For these particular stations, the frequency content of the source waves was broad enough to generate long-period oscillations at the coast. The spectrum of background oscillations at Salina Cruz contains two basic oscillation periods of about 75 and

18 min, while the tsunami spectrum contains numerous peaks at periods from 23 to 153 min. At Puerto Madero, the main background periods are 125 and 27 min, while the tsunami spectrum exhibits several peaks at periods between 153 and 12.5 min.

It is well known that the main spectral peaks for different tsunami events at the same site are very similar, while the spectral peaks from the same tsunami event but at different sites are substantially different (cf. Honda et al. 1908; Miller 1972; Rabinovich 1997). Figure 8, which shows tsunami spectra for six sites for the 2010 Chile and 2011 Tohoku events, illustrates this effect very clearly. The magnitudes of the two earthquakes were alike: $M_w = 8.8$ and $M_w = 9.0$, respectively. However, the source regions and, consequently, the directions of propagation were fundamentally different. The 2010 Chilean tsunami propagated along the Mexican coast from the southeast to the northwest (see Fig. 5 in Zaytsev et al. 2016), while the 2011 Tohoku tsunami wave spread toward Mexico in the opposite direction (i.e., from the northwest) (Fig. 5). Nevertheless, the spectra of these two tsunamis at each site are almost identical (Fig. 8). The coincidence of the spectra demonstrates the dominant influence of the local topography over the individual characteristics of the tsunami source.

3.4. Spectral Ratios (Source Functions)

Because of the dominating effect of near-shore bathymetry and coastal topography on arriving tsunami waves, it is problematic to reconstruct the spectral characteristics of the source based on data from coastal tide gauges. Rabinovich (1997) suggested a method to bypass this problem by separating the influences of topography and source on the observed tsunami spectrum. The method is based on the assumption that the transfer function, $W(\omega)$, describing the linear topographic transformation of long waves approaching the coast, is the same for the tsunami waves as for the ever-present background long waves. Specifically,

$$S_{\text{tsu},j}(\omega) = W_j(\omega) E_{\text{tsu},j}(\omega), \quad (2a)$$

$$S_{\text{bg},j}(\omega) = W_j(\omega) E_{0j}(\omega), \quad (2b)$$

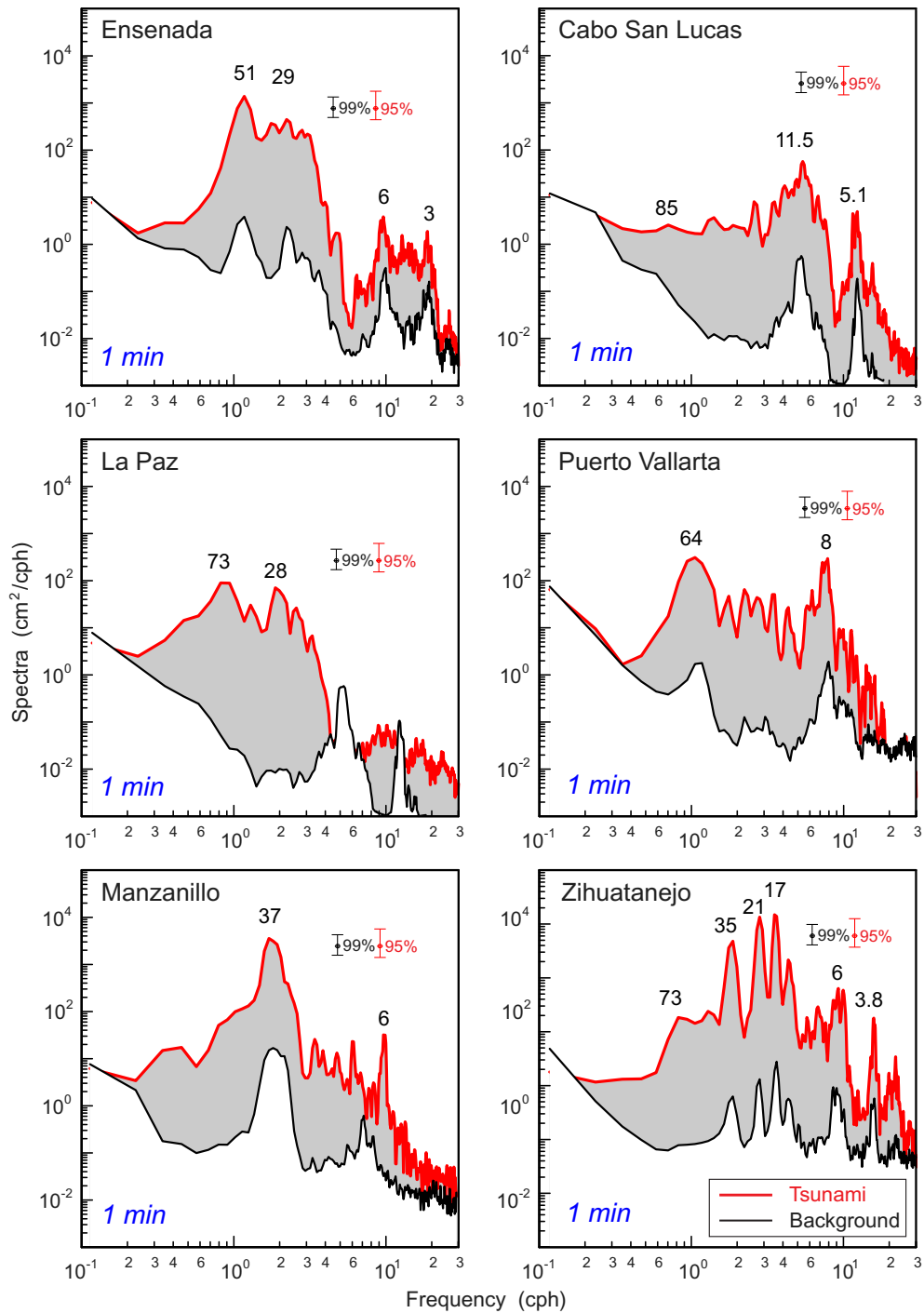


Figure 7

Spectra of background (pre-tsunami) and 2011 Tohoku tsunami sea-level oscillations for eight 1-min and four 6-min tide gauge records from the coast of Mexico. Periods (in min) of the main spectral peaks are indicated. The 95% confidence level applies to the tsunami spectra; the 99% confidence level to the background spectra. The shaded areas denote the tsunami energy

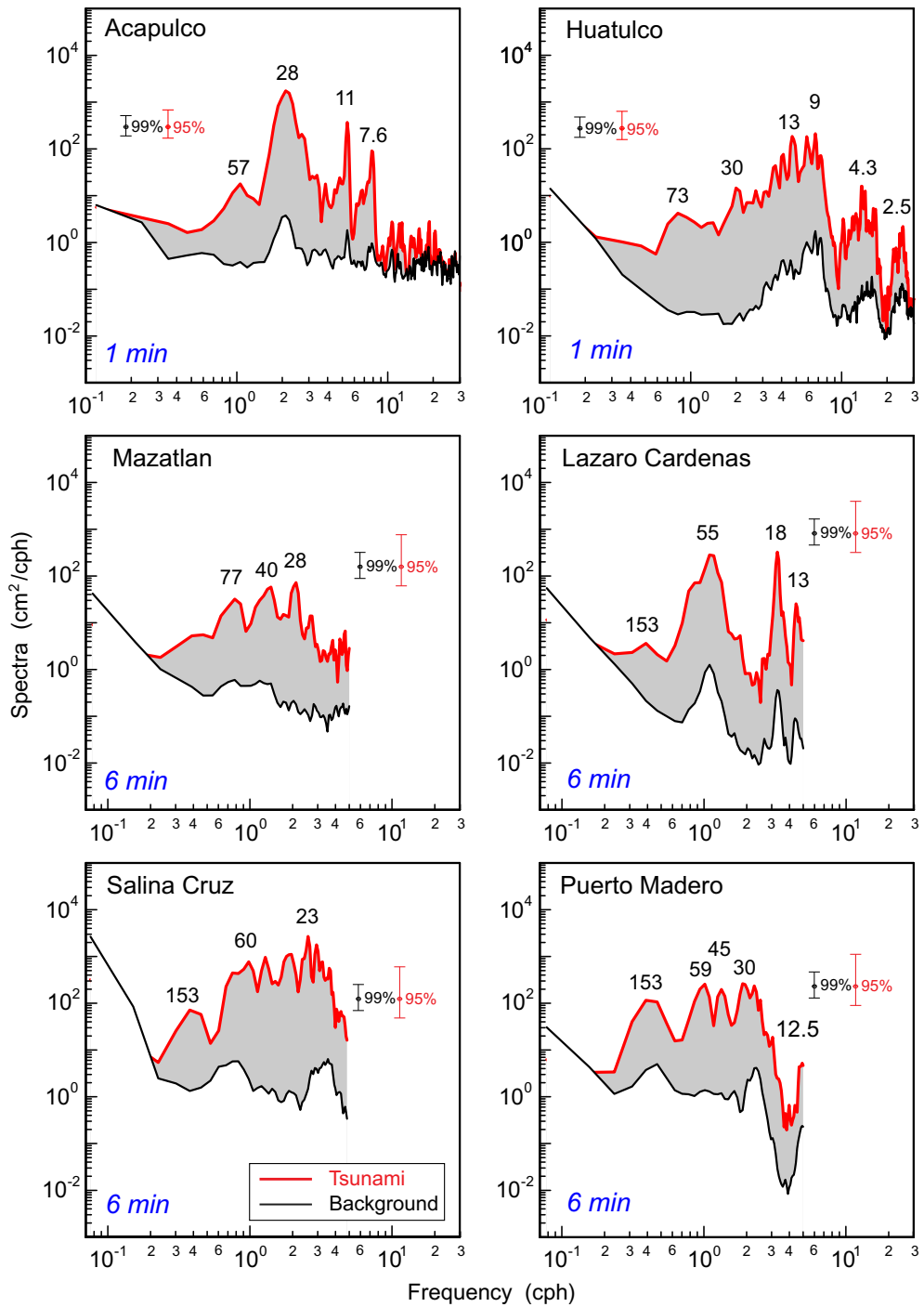


Figure 7 continued

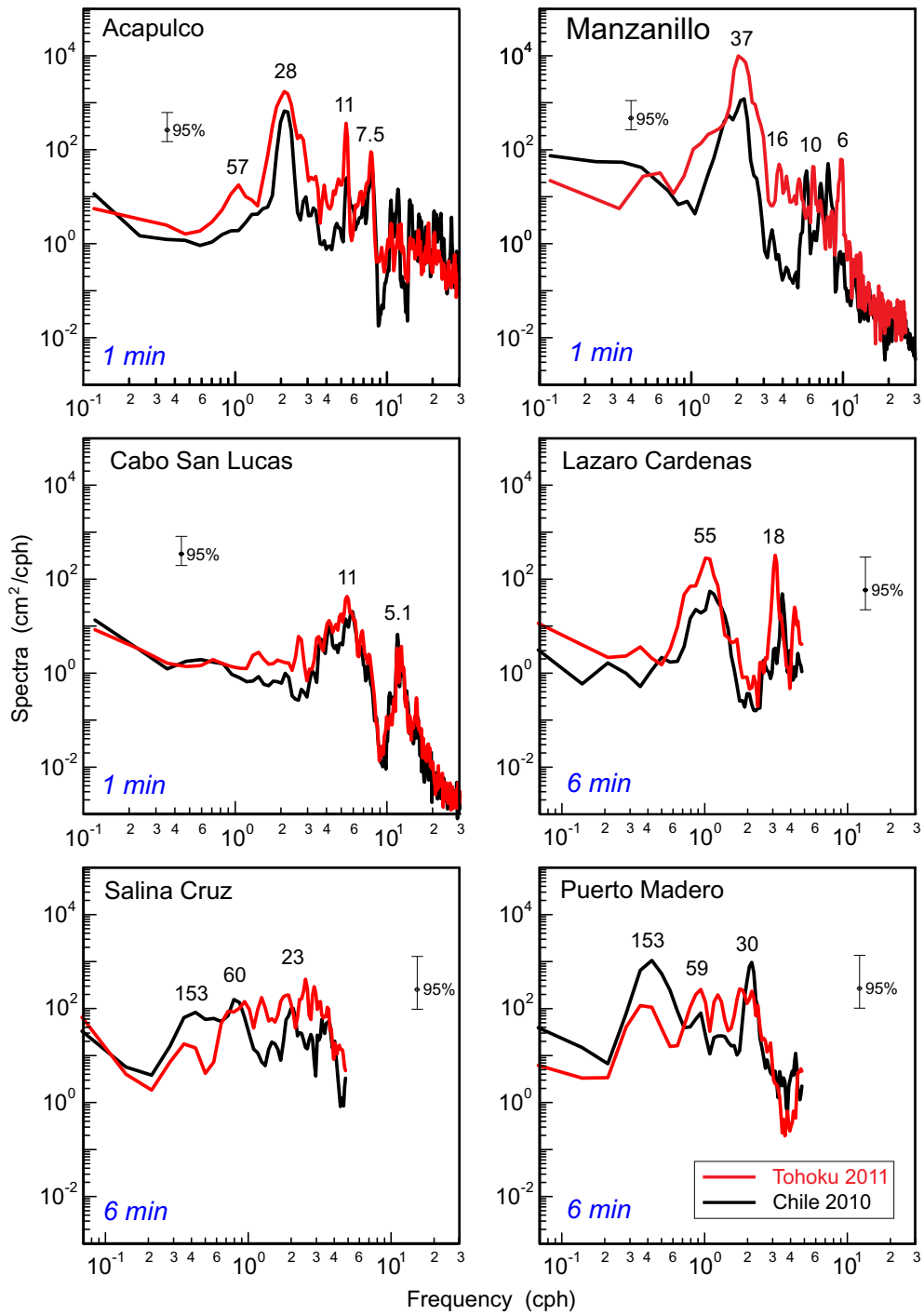


Figure 8

Spectra of the 2011 Tohoku tsunami compared to spectra of the 2010 Chile (Maule) tsunami for three 1-min and three 6-min tide gauge records on the coast of Mexico. Periods (in min) of the main spectral peaks are indicated

where $S_{\text{tsu},j}(\omega)$ and $S_{\text{bg},j}(\omega)$ are the tsunami and background spectra at the j th coastal site, and $E_{\text{tsu},j}(\omega)$ and $E_{0j}(\omega)$ are the respective spectra in the open ocean. The method assumes that individual characteristics of the observed spectra at the j th site are related to the site-specific topographic function, $W_j(\omega)$, while all general properties of the spectra are associated with the tsunami source. In other words, we assume that the function $W_j(\omega)$ is variable in space but almost uniform in time. Conversely, the corresponding source function $E_{\text{tsu},j}(\omega)$ is spatially uniform, $E_{\text{tsu},j}(\omega) \approx E_{\text{tsu}}(\omega)$, but varies with time (i.e., with different events) depending on the source parameters. In some ways, the methodology is similar to the harmonic expansion of tides, whereby the modulated amplitude of an individual n th tidal harmonic, A_n , is presented as a result of multiplication, such that $A_n = H_n f_n$, where H_n is the mean amplitude of the tidal harmonic, which is strongly variable in space but constant in time, and f_n is the nodal factor that is almost spatially uniform, but slowly changing in time over an 18.6 year period (Pugh and Woodworth 2014). Finally, we note that, based on numerous observations in the open ocean (cf. Kulikov et al. 1983; Filloux et al. 1991; Rabinovich and Eblé 2015), the background spectra, $E_{0j}(\omega)$, are uniform in space and constant in time, whereby $E_{0j}(\omega) \approx E_0(\omega)$.

According to (2), at each j th site, the ratio of the tsunami to the background spectrum,

$$R_{sj}(\omega) = S_{\text{tsu},j}(\omega)/S_{\text{bg},j}(\omega) = E_{\text{tsu},j}(\omega)/E_{0j}(\omega), \quad (3)$$

does not depend on local topographic features and is determined solely by the external forcing (i.e., by the characteristics of the open ocean tsunami waves). Although the true tsunami spectrum at the coast, $S_{\text{tsu},j}(\omega)$, is unknown, the observed coastal spectrum, $S_{\text{obs},j}(\omega)$, for sea-level oscillations is formed by the superposition of tsunami waves and background noise. Taking into account (2a), (2b), and (3), we can specify the “spectral source function”, i.e., the “spectral ratio” that quantifies the amplification of the tsunami spectrum relative to the background conditions:

$$R_j(\omega) = \frac{S_{\text{obs},j}(\omega)}{S_{\text{bg},j}(\omega)} = \frac{[E_{\text{tsu},j}(\omega) + E_{0j}(\omega)]}{\hat{E}_{0j}(\omega)} \approx R_{sj}(\omega) + 1.0, \quad (4)$$

where we have assumed that the open-ocean background spectrum before and during the event is approximately equal, such that $\hat{E}_{0j}(\omega) \approx E_{0j}(\omega)$. The individual spectral ratio function at the j th site, $R_j(\omega)$, is considered to be an invariant characteristic of the source and is expected to be nearly uniform at all stations within a specific region. The similarity of the function $R_j(\omega)$ at various stations validates the initial assumptions. The effectiveness of this method has been demonstrated for many tsunami events (cf. Rabinovich 1997; Vich and Monserrat 2009; Rabinovich et al. 2013a, b; Shevchenko et al. 2014) and was used by Zaytsev et al. (2016) to examine the spectral properties of the 2010, 2014, and 2015 Chilean tsunamis on the coast of Mexico. The results were quite consistent, especially, for the 2010 tsunami, the strongest of the three events.

Figure 9 presents the spectral ratios derived from the 12 tide gauge spectra shown in Fig. 7. In contrast to the individual spectra, which are significantly different from each other and have different resonant peaks, the source functions calculated for the various sites are much more similar and do not have specific peaks related to coastal topographic resonance (which are evident in the tsunami spectra shown in Figs. 7 and 8). In general, the source functions have a characteristic “dome-like” shape, typical for great tsunamis (cf. Rabinovich et al. 2013; Zaytsev et al. 2016) and occupy a wide frequency band from about 0.2 to 30 cph (periods from 5 h to 2 min). The maximum values of $R_j(\omega)$ are related to frequencies 1.5–2.0 cph (i.e., to periods of 30–40 min). The estimated ratios are in reasonable agreement with each other and, therefore, represent the general spectral properties of the source. The maximum amplification of the tsunami waves relative to the background noise (>1000 times) occurs at Ensenada, Cabo San Lucas, Manzanillo, and Zihuatanejo. The mean values of $R_j(\omega)$ integrated over the entire frequency band ranges from ~ 18 at La Paz to ~ 98 at Cabo San Lucas. The overall mean tsunami amplification relative to the background noise for

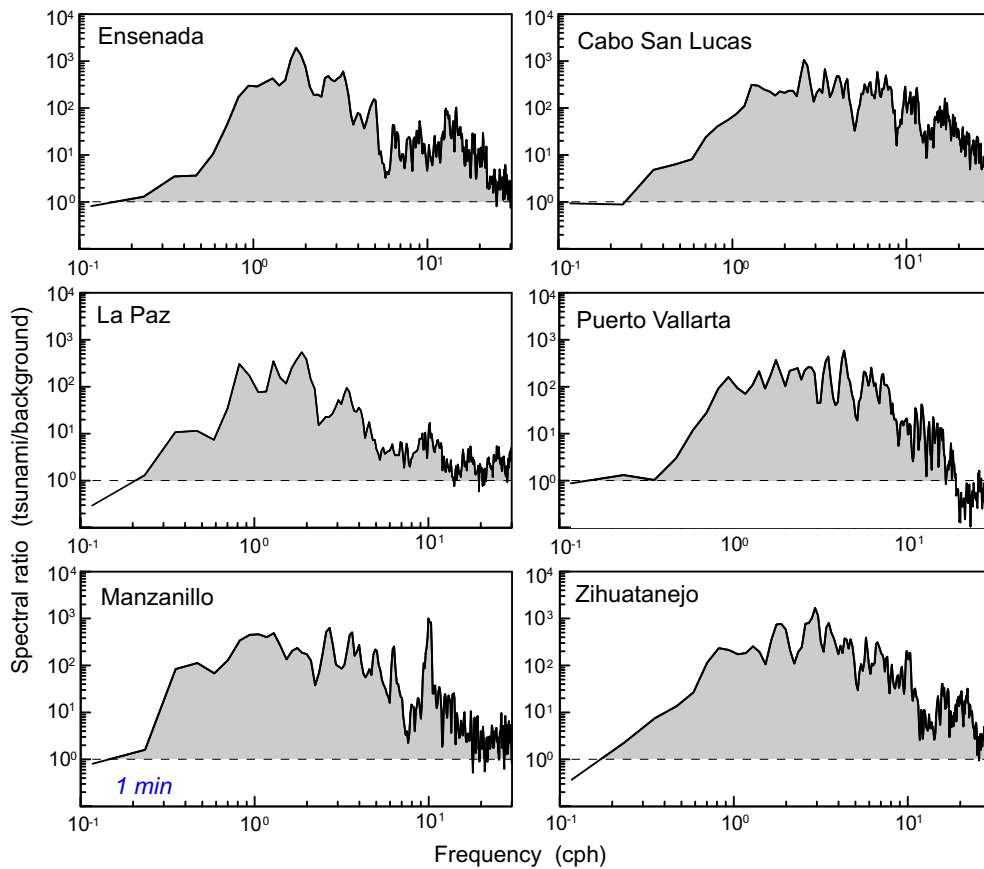


Figure 9

Ratios of the tsunami spectra to the background spectra for the 12 coastal tide gauge spectra shown in Fig. 7. The shaded areas denote the tsunami response associated with the arriving waves, i.e., the amplification of spectra due to the tsunami waves measured relative to the background spectra

the 2011 Tohoku tsunami on the Mexican coast is 57. For comparison, the amplification for the 2010 Chile tsunami was 48 on this coast, which is about 16% smaller, likely due to the fact that the 2010 tsunami was weaker than the 2011 tsunami.

4. Open-Ocean Tsunami Spectra

Open-ocean Bottom Pressure Recorders (BPRs) are not affected by various coastal effects and have very low background noise in comparison with coastal tide gauges. As a consequence, BPRs provide the most accurate and precise information about tsunami waves that can be effectively used for early tsunami warning (cf. Titov 2009; Thomson et al.

2013; Tang et al. 2012), but also to investigate physical characteristics of the source region and specific properties of propagating tsunami waves (Mofjeld 2009; Rabinovich and Eblé 2015). Long series of high-quality and high temporal resolution data downloaded from retrieved instruments allow us to estimate precisely the open-ocean spectral properties of tsunami waves and background oscillations (Rabinovich et al. 2013a, b; Titov et al. 2016). To examine these properties for the 2011 Tohoku tsunami off the Mexican coast, we were able to use 15-s data from two DART stations, 46412 and 43413 (Fig. 2; Table 1).

Spectral analysis of the 46412 and 43413 records followed the same procedure as for the coastal data (Sect. 3.3) and for analysis of the 2010 Chile tsunami

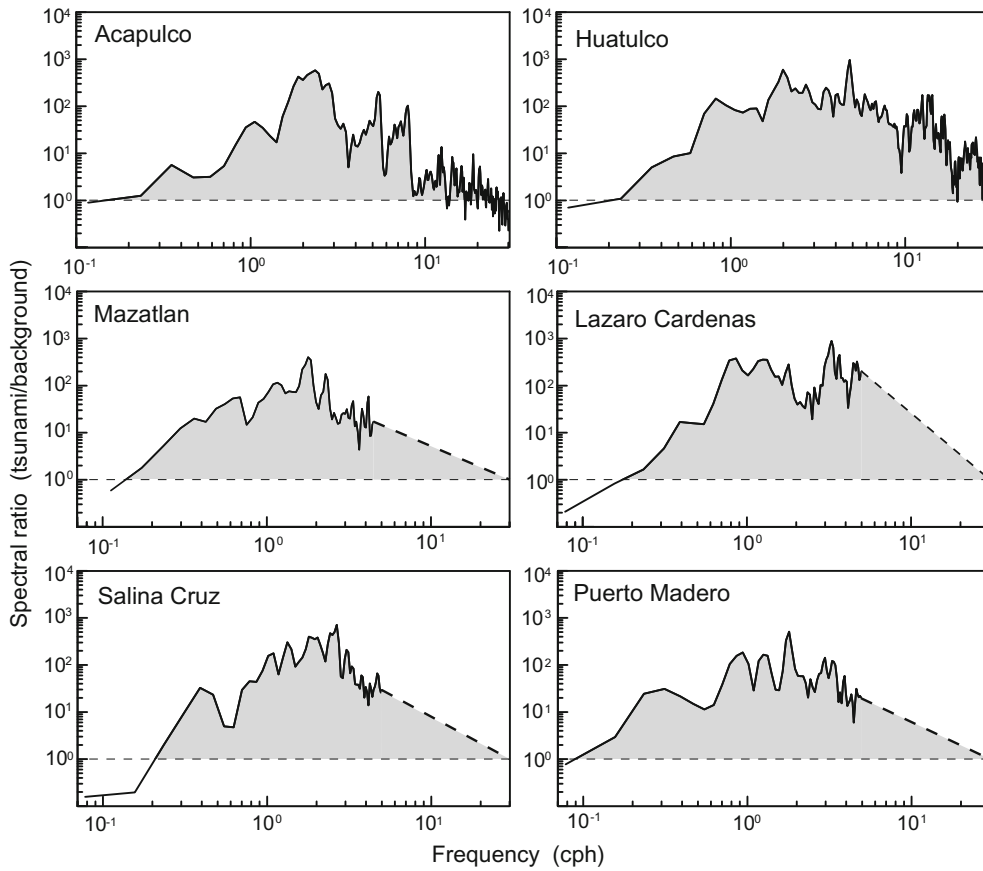


Figure 9
continued

(Zaytsev et al. 2016). To estimate background spectra, we used 6-day records immediately prior to the tsunami (33,792 values of 15-s data), while for the tsunami spectra, we used 34-h segments (8192 values). The length of the KB window was chosen to be 512 min, yielding $\nu = 64$ degrees of freedom for the background spectra and $\nu = 14$ for the tsunami spectra. The spectral resolution for all spectra was $\Delta f \approx 0.117$ cph and the Nyquist frequency $f_n = 120$ cph. The computed tsunami and background spectra for DARTs 46412 and 43413 are shown in Fig. 10. The observed tsunami spectra at the two sites are similar, occupy a wide frequency band from 0.25 to 40 cph (periods from 4 h to 1.5 min), and do not have the well-defined peaks that are typical of coastal observations. The tsunami spectra exceed the background spectra by 2–3 orders of magnitude. At a frequency of about 20 cph (3 min), the tsunami

spectrum drops sharply to “white noise” (instrumental noise) at a frequency of roughly 40 cph.

The main feature of the background spectra is their pronounced similarity, indicating that in the deep ocean, where the topographic effects are negligible, there is high spatial homogeneity of the open-ocean wave field (Rabinovich and Eblé 2015). In a wide band of frequencies, from 0.4 to 6–8 cph, the long-wave spectrum, $E_0(\omega)$, is well described by the power law ω^{-2} (Fig. 10), whereby

$$E_0(\omega) = A_0 \omega^{-2.0}. \quad (5)$$

The universal character of this law for open-ocean long-wave spectra has been confirmed by numerous observations in various regions of the Pacific Ocean (cf. Kulikov et al. 1983; Filloux et al. 1991; Rabinovich 1997). The prominent spectral “bulge” at frequencies 10–50 cph (periods 6–1.2 min) is an

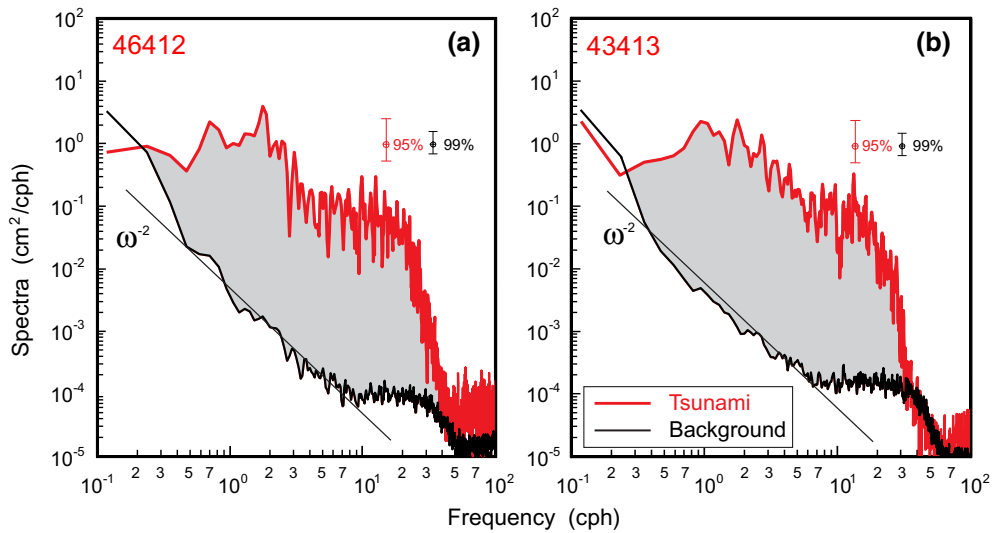


Figure 10

Spectra of the open-ocean sea-level records for the background (pre-tsunami) and the 2011 Tohoku tsunami oscillations for DARTs **a** 46412 and **b** 43413. The shaded areas denote the tsunami energy. The 95% confidence level applies to the tsunami spectra; the 99% confidence level to the background spectra. The solid black line indicates the theoretical spectral power law, ω^{-2} , for open-ocean background spectra

artefact associated with infragravity (IG) waves generated by nonlinear interaction of wind waves or swell for frequencies >6 cph (Webb et al. 1991; Rabinovich 1993, 2009), while at higher frequencies, when wave lengths, λ , become short compared with the water depth h , the spectra rapidly attenuate as $1/\cosh(kh)$, where $k = 2\pi/\lambda$ is the wavenumber (Rabinovich and Eblé 2015). Recently, Aucan and Ardhuin (2013) considered this problem in detail based on DART data.

The “true” (unaltered) tsunami spectrum in the open ocean can be easily estimated as the difference between the observed and background spectra from the DART records: specifically,

$$E_{\text{tsu}}(\omega) = E_{\text{obs}}(\omega) - E_0(\omega). \quad (6)$$

The true tsunami spectra for DARTs 46412 and 43413 are shown in Fig. 11 (black line). The spectra are very similar, with most of the tsunami wave energy concentrated at relatively low frequencies of 0.3–3.0 cph (periods from 3.3 h to 20 min). For frequencies above 20 cph (2 min), the spectra attenuate rapidly. There are two minor peaks in the spectra at frequencies 0.7–0.9 (periods of 65–85 min) and 1.7 cph (35 min).

Zaytsev et al. (2016) demonstrated that the true open-ocean tsunami spectra, $E_{\text{tsu},j}(\omega)$, can be

evaluated from the coastal observations. Using (4), we can express these spectra in the form:

$$E_{\text{tsu},j} = [R_j(\omega) - 1.0] E_0(\omega), \quad (7)$$

where $R_j(\omega)$ is the spectral ratio estimated for a specific coastal site. Thus, if $E_0(\omega)$ is known from the offshore measurements, we can use (7) to reconstruct the “individual” open-ocean spectral characteristics of tsunami waves, $E_{\text{tsu},j}(\omega)$, based on coastal ratios, $R_j(\omega)$, from various sites or from the mean ratio values, $\hat{R}(\omega)$.

We used two approaches to reconstruct $E_{\text{tsu},j}(\omega)$ from coastal measurements. The first approach is based on expression (5), where $E_0(\omega)$ is approximated by $A_0\omega^{-2.0}$, and where $A_0 = 4 \times 10^{-3} \text{ cm}^2/\text{cph}$, as estimated from the DART background spectra. The second approach is to use the spectrum of $E_0(\omega)$ determined from the observations at the specific DART site. As shown in Fig. 11, the agreement between the actual (observation-based) and reconstructed tsunami spectra at frequencies <5 cph (at periods >12 min) is very good for both DART sites. Not only do absolute values match, but also even some small spectral details match, including minor spectral peaks and troughs. Equally importantly, most of tsunami energy is specifically related to the <5 cph frequency band. At higher frequencies

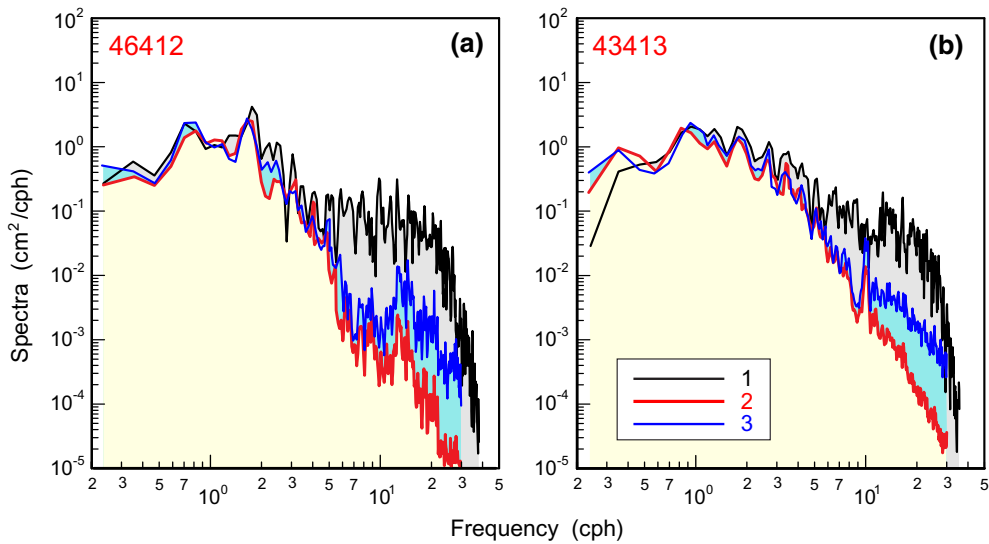


Figure 11

Tsunami spectra for **a** northern DART site 46412 and **b** southern DART site 43413. The *black line* (1) denotes the “true” open-ocean tsunami spectra; the *red lines* (2) are the reconstructed tsunami spectra based on the “northern” and “southern” coastal tide gauge records and the assumed $S \sim \omega^{-2}$ power law. The *blues lines* (3) are the reconstructed tsunami spectra based on the actual open-ocean background spectra

(>5 cph), the actual and reconstructed tsunami spectra begin to diverge. The reason of this effect is discussed in the next section.

Following Zaytsev et al. (2016), we integrated the true tsunami spectra (Fig. 11) over the entire tsunami frequency band, $\omega_{begin} < \omega < \omega_{end}$, and estimated the *integral open-ocean tsunami energy*, I_0 :

$$I_0 = \int_{\omega_{begin}}^{\omega_{end}} E_{tsu}(\omega) d\omega. \quad (8)$$

This parameter, which is evaluated from open-ocean tsunami measurements, is independent of local bathymetric or topographic effects and may be considered as a fundamental property of open-ocean tsunami waves. We emphasise that, in the present study, this parameter was calculated using 1.5 days of tsunami observations. As a result, the parameter characterises the steady-state stage of these waves, after they had become well diffused over the Pacific Ocean (cf. Van Dorn 1984), rather than the initial propagation phase of the waves.

Figure 12a shows the parameter I_0 directly estimated from true open-ocean spectra for the 2011 Tohoku tsunami. As indicated, the values for the two DARTs are nearly identical: 2.29 cm² (46412) and

2.33 cm² (43413). The same parameter was also derived from “reconstructed” tsunami spectra based on coastal measurements (blue lines in Fig. 11). Here, we have presented the spectral ratio estimated for Ensenada, the northernmost coastal station nearest to DART 46412, as well as the “*mean spectral ratio*”. $\hat{R}(\omega)$, evaluated by averaging $R_j(\omega)$ for a group of six southern stations. The results (Fig. 12b) show that the “reconstructed” values of I_0 , 2.54 and 2.74 cm², respectively, are only slightly (13–17%) larger than “true” values.

In addition to the absolute values of I_0 , represented by the *circle areas* in Fig. 12, we also estimated the *tsunami colour*, a measure of the open-ocean frequency content of each tsunami. The entire tsunami frequency band, $\omega_{begin} < \omega < \omega_{end}$, was separated into seven partitions (see the legend in Fig. 12), and for each of these partitions, we estimated the respective energy contribution (band variance). As revealed in Fig. 12, the 2011 Tohoku tsunami was “reddish”, where circles with red colour denote the prevalence of low frequencies. In this case, approximately 65% of the total energy is at frequencies <1.7 cph, i.e., at long periods from 205 to 35 min. The colours of “true” and “reconstructed” circles (Fig. 12a, b) agree well, except that the percentage of

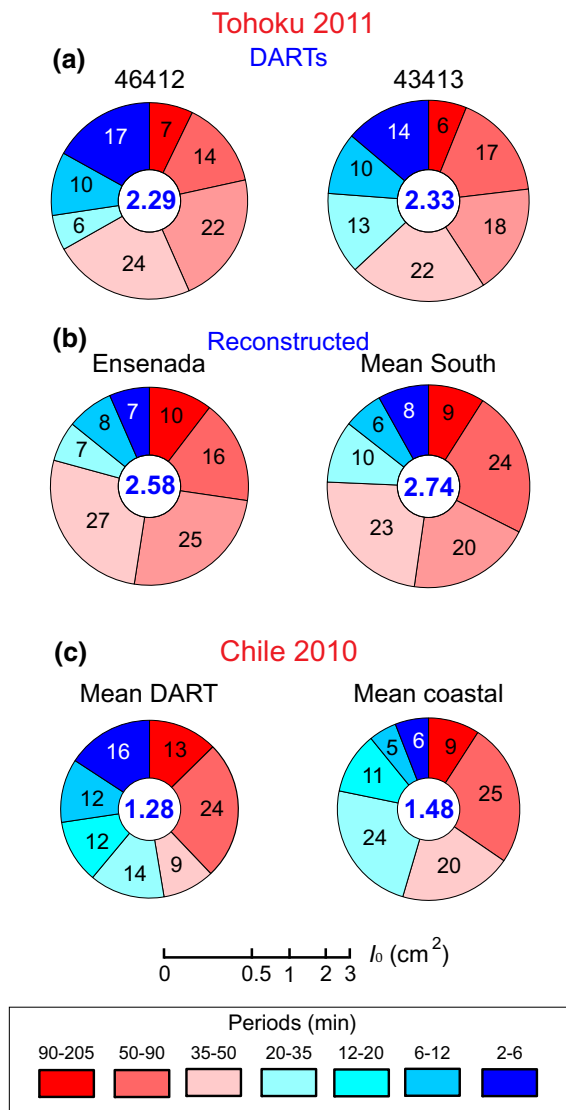


Figure 12

a Integral, open-ocean tsunami energy, I_0 , for the 2011 Tohoku tsunami estimated from the “true” spectra (in this figure) for DART 46412 (left) and DART 43413 (right); **b** “reconstructed” values of I_0 for DART 46412 (left), derived using the coastal tsunami/background ratio at Ensenada, and for DART 43413 (right) using the mean coastal ratio for the four “southern” sites (Manzanillo, Zihuatanejo, Acapulco, and Huatulco); and **c** the mean integral open-ocean tsunami energy, I_0 , for the 2010 Chilean tsunami averaged using the “true” tsunami spectra at DARTs 46412 and 43413 (left) and the reconstructed value of I_0 from the mean coastal ratio at six sites (right) (see Zaytsev et al. 2016). The area of a circle is proportional to $\text{Log}(I_0)$. The different coloured segments in circle denote different period partitions shown as indicated in the legend

high-frequency (“bluish”) energy is noticeably smaller for circles denoting the reconstructed spectra.

The “true” values of I_0 and the mean variance of tsunami waves on the coast, $\text{Var}_0 = 451 \text{ cm}^2$ (see Sect. 3.1), can be used to estimate the relative amplification of tsunami waves,

$$A = \sqrt{\text{Var}_0/I_0}, \tag{9}$$

as they arrive at the coast. For the 2011 Tohoku tsunami on the Mexican coast, we find $A = 13.9\text{--}14.0$. Comparable values of A were estimated by Zaytsev et al. (2016) for the three Chilean tsunamis: 14.3 (2010), 20.3 (2014), and 24.3 (2015). We assume that the main factor influencing this parameter is the *general amplification* properties for this region. At the same time, it is evidently that actual spectral properties for various events can substantially affect this parameter. Similar amplification parameters can be estimated for individual parameters can be estimated for individual sites, but it is obvious that these would be much more variable for different events depending on resonant properties and Q -factor of a particular site and on the dominant frequencies of the incoming waves.

It is of interest to compare the open-ocean parameters for the 2011 Tohoku and 2010 Chile great tsunamis (Figs. 12a–c, respectively). The integral open-ocean tsunami energy, I_0 , for the 2011 event was approximately 1.7 times larger than for the 2010 event, which is to be expected considering the larger magnitude of the former earthquake ($M_w = 9.0$ vs 8.8). Both tsunamis were “red” (predominantly low-frequency), but the percentage of long-period motions with periods >35 min for the 2011 tsunami was noticeably higher. In general, the “red colour” (i.e., the prevalence of low-frequency waves in both tsunamis), is explained by the large extension of the source regions. In contrast, the 2014 and 2015 Chilean earthquakes had much smaller source regions and, consequently, induced “bluish” tsunamis (Zaytsev et al. 2016).

5. Discussion

One of the questions that arose from our study is: *Why do the “true” and “reconstructed” open-ocean*

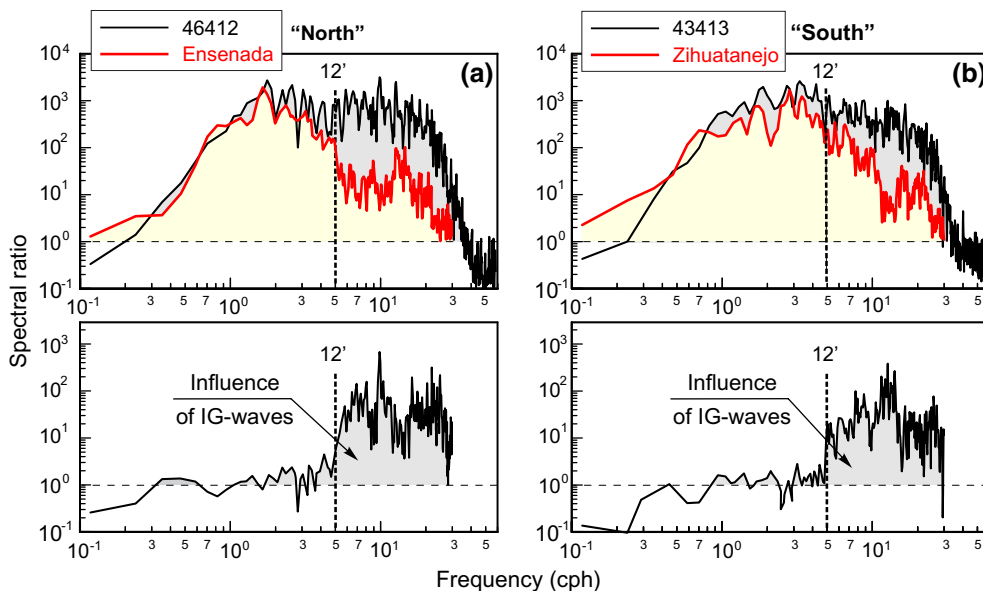


Figure 13

a Top tsunami/background spectral ratios for DART 46412 and Ensenada; *Bottom* the “ratio of these two ratios”, i.e., the ratio 46412/Ensenada; **b** the same as **a** but for DART 43413 and Zihuatanejo. *Shaded areas* denote the difference between open-ocean and coastal ratios that we assume those are due to the contribution from *infragravity (IG) waves* generated in the coastal zone by the incoming tsunami. The *dashed vertical black lines* indicate the period of 12 min, the assumed low-frequency limit of IG-wave influence

tsunami spectra perfectly coincide at low frequencies but diverge at higher frequencies? This question is important as it addresses some basic differences between tsunami waves observed in the open ocean versus those observed near the coast.

It is evident from Fig. 13a that the difference between the “true” tsunami spectra and the “reconstructed” spectra (black and blue lines, respectively, in Fig. 11) is related to the difference in $R_j(\omega)$ estimated from coastal and open-ocean spectra. For frequencies <5 cph (periods >12 min), the open-ocean and coastal tsunami/background spectral ratios match each other fairly well. However, above this frequency, the “coastal” ratios abruptly decrease, while “open-ocean” ratios remain approximately the same (at least, for frequencies <20 cph; periods >3 min). To further illustrate this effect, we constructed “ratios of ratios” (Fig. 13b). The plots reveal a sharp transition at around 5 cph between two frequency regimes; the “spectrally similar” and “spectrally dissimilar”. We also note that independent measurements at two sites located about 3200 km apart give very similar results, indicating that the observed effect is not related to local

properties of a specific region but to a general physical mechanism associated with the tsunami wave field generation.

The differences between $R_{\text{coast}}(\omega)$ and $R_{\text{ocean}}(\omega)$ (Fig. 13) indicate that

$$W_{\text{bg}}(\omega) \neq W_{\text{tsu}}(\omega) \quad (10)$$

at $\omega/2\pi \geq 5$ cph, where according to (2a, 2b), $W_{\text{bg}}(\omega)$ and $W_{\text{tsu}}(\omega)$ are the background and tsunami topographic transfer functions, respectively. Such an abrupt frequency-dependent change in the transfer function is atypical of linear systems. However, we can account for the dissimilarity between $W_{\text{bg}}(\omega)$ and $W_{\text{tsu}}(\omega)$ at high frequencies (HF) by noting that the effect is not due to differences in the transformation of shoreward propagating tsunami and background waves, but to the presence of long HF background waves generated on the continental shelf and in the near-shore zone. The most obvious type of long near-shore waves is *infragravity (IG) waves*, also known in the coastal zone as *surf beat* (Munk 1949; Rabinovich 1993, 2009). Typical periods of these waves, which are formed by the nonlinear interaction of wind waves or swell, are from 30 to

300 s, but they can achieve much larger periods, especially during major storms (Kovalev et al. 1991). Of particular relevance to the present study is that the effectiveness of IG-wave generation strongly depends on the water depth: the smaller the depth, the more intense the IG generation and the larger the wave heights. In general, the empirical relationship between IG-wave height (H_{IG}), significant wave height for the wind waves or swell (H_s), and the water depth (h) is roughly given by

$$H_{IG} = \delta H_s^\gamma h^{-1/2} \quad (11)$$

(Rabinovich 1993), where $\delta = 0.23$ and $\gamma = 1.5$ – 2.0 .

Infragravity waves are prevalent in sea-level records throughout the World Ocean. As indicated in Sect. 3.3, these waves are responsible for the high-frequency “bulge” in open-ocean spectra (Fig. 10; see also Aucan and Ardhuin 2013; Rabinovich and Eblé 2015). In the open ocean, the waves are small and rarely exceed 0.5 cm (cf. Webb et al. 1991; Rabinovich and Eblé 2015); however, in coastal regions, the heights of IG waves can exceed several tens of centimetres. Unlike tsunami waves, which are *free waves* that amplify toward the shore according to the Green’s law (i.e., H_{tsu} is proportional to $h^{-1/4}$; cf. Pelinovsky 2006), IG waves in the open ocean are mainly *forced waves* that are bound to wind wave groups. The heights of these *bound waves* (also known as *locked waves*; cf. Rabinovich 1993, 2009) increase in the onshore direction according to (11) (i.e., much more rapidly than tsunami waves). As demonstrated by Longuet-Higgins and Stewart (1962, 1964), who established the theory of IG waves, IG-wave heights in the near-shore zone increase not as $h^{-1/2}$, as follows from (11), but even much more rapidly. As a result, during strong storms, IG heights near the coast can exceed 1–1.5 m.

Most of coastal tide gauges are located in bays and harbours, which shelter the gauges from the direct impact of storm waves and associated forced IG waves. However, after wave breaking, reflection, and other processes in the coastal zone, the energy of forced IG waves is transferred into *free IG waves* (edge and leaky waves). A substantial fraction of this energy penetrates into the harbour,

increasing the background noise level (Rabinovich 2009). Consequently, the signal-to-noise ratio for coastal records (here, the ratio of tsunami to background waves in the IG frequency band) is much smaller than in open-ocean records. As is evident in Fig. 13, this process needs to be taken into account when correcting the “reconstructed” open-ocean spectra, but this is being a subject for future study.

6. Conclusions

The Tohoku (East Japan) earthquake of 11 March 2011 (M_w 9.0) generated a highly destructive trans-Pacific tsunami that was recorded by 14 tide gauges along the coast of Mexico. The event was the strongest tsunami on this coast since the Alaska earthquake and tsunami of 1964. Maximum trough-to-crest wave heights were observed at Manzanillo (258 cm), Zihuatanejo (258 cm), Ensenada (190 cm), Acapulco (187 cm), and Huatulco (126 cm). These sites were also the locations of maximum wave heights for the 2010, 2014, and 2015 Chilean tsunamis (Zaytsev et al. 2016), which were identified and mapped as “hot” tsunami impact sites for the Mexican coast. The results for the 2011 tsunami confirm these sites as having higher potential tsunami hazard for major trans-oceanic tsunamis. In contrast, such sites as Topolobampo (13 cm), San Carlos (20 cm), Mazatlan (43 cm), and La Paz (52 cm) may be considered as “cold” sites, i.e., sites with lower tsunami risk. Lazaro Cardenas is located between two “hot” spots (Acapulco and Manzanillo), but has much smaller maximum wave height (95 cm). This might be explained by regional slope topography and the fact that the Lazaro Cardenas tide gauge is located in a sheltered harbour. In general, it is clear that tsunami waves at “hot” sites are significantly amplified by topographic features, while “cold” sites are shielded from incoming tsunami waves resulting in their strong attenuation.

This study has combined coastal and open-ocean tsunami measurements and used the spectral analysis methodology suggested by Zaytsev et al. (2016) to estimate the “true” deep-ocean tsunami spectra based on the analysis of DART data. We have also used

coastal tide gauge data to “reconstruct” the open-ocean spectra of the tsunami waves. Except for the high-frequency (>5 cph) spectral band where spectra diverge, the reconstructed open-ocean tsunami spectra are in good agreement with the true tsunami spectra evaluated from direct analysis of DART records collected off the Mexican coast. We show that this divergence is due to the contribution to the wave spectra from background infragravity waves generated in the coastal zone.

We have further used the spectral estimates to parameterize the energy of the 2011 Tohoku tsunami based on the total open-ocean tsunami energy. The tsunami frequency band for the 2011 event was wide: from 0.25 to 40 cph (periods from 4 h to 1.5 min), approximately the same as was for the 2010 Chile tsunami. The integral open-ocean tsunami energy, I_0 , estimated from DARTs 46412 and 43413 for the entire tsunami frequency band was $\sim 2.30 \text{ cm}^2$, or approximately 1.7 times larger than was observed at the same DARTs for the 2010 event. Comparison of this parameter with the mean tsunami variance at the coastal sites (451 cm^2) indicates that tsunami waves propagating onshore from the open ocean amplified by 14 times; the same value of amplification parameter was obtained by Zaytsev et al. (2016) for the 2010 Chilean tsunami.

Zaytsev et al. (2016) introduced another crucial characteristic of tsunami events: the “tsunami colour” (frequency content), in analogy with classical light spectrum. Tsunamis range from red (mainly low-frequency) to blue (mainly high-frequency). The results for the 2011 Tohoku tsunami indicate that the 2011 Tohoku tsunami was “red”, with about 65% of the total energy associated with low-frequency waves at frequencies <1.7 cph (periods >35 min). Such long periods appear to be related to the large extension of the 2011 source area.

The close agreement between open-ocean tsunami parameters estimated from observation-derived open-ocean tsunami spectra with those obtained from “reconstructed” coastal spectra supports the analytical approaches developed by Zaytsev et al. (2016) to examine three Chilean tsunamis and to demonstrate that they enable us to reliably reproduce open-ocean tsunami parameters based on coastal tsunami wave measurements.

Acknowledgements

This work was partially supported by the Mexican Instituto Politécnico Nacional (IPN, Project SIP 20171223). Additional support for the first author was provided by SNI (Mexican National System of Investigators). For ABR, this study was partly supported by the RSF Grant 14-50-00095. We gratefully acknowledge the Mexican National Mareographic Service of the UNAM and the Laboratory of the Sea Level of the CICESE for providing us the coastal sea-level data and George Mungov (NOAA/NCEI, Boulder, Colorado) for assisting us with the DART data. We sincerely thank Isaac Fine (IOS, Sidney, BC) for useful discussions and for providing us the results of numerical modeling of the 2011 Tohoku tsunami, Paul Whitmore and Christopher Popham (NTWC, Palmer, AK) for presenting us precise ETAs for the tsunamis recorded by DARTs 46412, 43412, and 43413 offshore of Mexico, and Maxim Krassovski (IOS, Sidney, BC) for helping us with the figures.

REFERENCES

- Admiral, A., Dengler, L., Crawford, G., Uslu, B., Borrero, J., Greer, D., et al. (2014). Observed and modeled currents from the Tohoku-oki, Japan and other recent tsunamis in northern California. *Pure and Applied Geophysics*, 171(12), 3403–3485. doi:10.1007/s00024-014-0797-8.
- Aoyama, M., Hamajima, Y., Hult, M., Uematsu, M., Oka, E., Tsumune, D., et al. (2016a). ^{134}Cs and ^{137}Cs in the North Pacific Ocean derived from the March 2011 TEPCO Fukushima Dai-ichi nuclear power plant accident, Japan. Part one: surface pathway and vertical distributions. *Journal of Oceanography*, 72(1), 53–65. doi:10.1007/s10872-015-0335-z.
- Aoyama, M., Kajino, M., Taichu, Tanaka, T. Y., Sekiyama, T. T., Tsumune, D., et al. (2016b). ^{134}Cs and ^{137}Cs in the North Pacific Ocean derived from the March 2011 TEPCO Fukushima Dai-ichi nuclear power plant accident, Japan, 2015b. Part two: estimation of ^{134}Cs and ^{137}Cs inventories in the North Pacific Ocean. *Journal of Oceanography*, 72(1), 67–76. doi:10.1007/s10872-015-0332-2.
- Aucan, J., & Ardhuin, F. (2013). Infragravity waves in the deep ocean: An upward revision. *Geophysical Research Letters*, 40, 3435–3439. doi:10.1002/grl.50321.
- Borrero, J. C., Bell, R., Csato, C., DeLange, W., Goring, D., Greer, S. D., et al. (2013). Observations, effects and real time assessment of the March 11, 2011 Tohoku-oki tsunami in New Zealand. *Pure and Applied Geophysics*, 170(6–8), 1229–1248. doi:10.1007/s00024-012-0492-6.
- Borrero, J. C., & Greer, S. D. (2013). Comparison of the 2010 Chile and 2011 Japan tsunamis in the far field. *Pure and Applied*

- Geophysics*, 170(6–8), 1249–1274. doi:[10.1007/s00024-012-0559-4](https://doi.org/10.1007/s00024-012-0559-4).
- Buesseler, K., Dai, M., Aoyama, M., Benitez-Nelson, C., Char-masson, S., Highley, K., et al. (2017). Fukushima Daiichi-derived radionuclides in the ocean: Transport, fate, and impacts. *Annual Reviews in Marine Science*, 9, 173–203.
- Candella, R. N., Rabinovich, A. B., & Thomson, R. E. (2008). The 2004 Sumatra tsunami as recorded on the Atlantic coast of South America. *Advances in Geosciences*, 14(1), 117–128.
- Eblé, M. C., Mungov, G., & Rabinovich, A. B. (2015). On the leading negative phase of major 2010–2014 tsunamis. *Pure and Applied Geophysics*, 172(12), 3493–3508. doi:[10.1007/s00024-015-0111-1](https://doi.org/10.1007/s00024-015-0111-1).
- Filloux, J. H., Luther, D. S., & Chave, A. D. (1991). Update on sea floor pressure and electric field observations from the north-central and north-eastern Pacific: Tides, infratidal fluctuations, and barotropic flow. In B. B. Parker (Ed.), *Tidal Hydrodynamics* (pp. 617J–639J). New York: J. Wiley.
- Fine, I. V., Kulikov, E. A., & Cherniawsky, J. Y. (2013). Japan's 2011 tsunami: Characteristics of wave propagation from observations and numerical modelling. *Pure and Applied Geophysics*, 170(6–8), 1295–1307. doi:[10.1007/s00024-012-0555-8](https://doi.org/10.1007/s00024-012-0555-8).
- Fine, I. V., & Thomson, R. E. (2013). A wave front orientation method for precise numerical determination of tsunami travel time. *Natural Hazards and Earth System Sciences*, 13, 2863–2870. doi:[10.5194/nhess-13-2863-2013](https://doi.org/10.5194/nhess-13-2863-2013).
- Heidarzadeh, M., & Satake, K. (2013). Waveform and spectral analyses of the 2011 Japan tsunami records on tide gauge and dart stations across the Pacific Ocean. *Pure and Applied Geophysics*, 170(6–8), 1275–1293. doi:[10.1007/s00024-012-0558-5](https://doi.org/10.1007/s00024-012-0558-5).
- Hinwood, J. B., & McLean, E. J. (2013). Effects of the March 2011 Japanese tsunami in bays and estuaries of SE Australia. *Pure and Applied Geophysics*, 170(6–8), 1207–1227. doi:[10.1007/s00024-012-0561-x](https://doi.org/10.1007/s00024-012-0561-x).
- Honda, K., Terada, T., Yoshida, Y., & Isitani, D. (1908). An investigation on the secondary undulations of oceanic tides. *Journal of the College of Science, Imperial University of Tokyo*, p. 108.
- Kovalev, P. D., Rabinovich, A. B., & Shevchenko, G. V. (1991). Investigation of long waves in the tsunami frequency band on the southwestern shelf of Kamchatka. *Natural Hazards*, 4(2/3), 141–159.
- Kulikov, E. A., Rabinovich, A. B., Spirin, A. I., Poole, S. L., & Soloviev, S. L. (1983). Measurement of tsunamis in the open ocean. *Marine Geodesy*, 6(3–4), 311–329.
- Longuet-Higgins, M. S., & Stewart, R. W. (1962). Radiation stress and mass transport of gravity waves, with application to “surf-beats”. *Journal of Fluid Mechanics*, 13(4), 481–504.
- Longuet-Higgins, M. S., & Stewart, R. W. (1964). Radiation stress in water waves: a physical discussion with applications. *Deep-Sea Research*, 11(4), 529–562.
- Miller, G. R. (1972). Relative spectra of tsunamis. *Hawaii Institute of Geophysics*, HIG-72-8, p. 7.
- Mofjeld, H. O. (2009). Tsunami measurements. In: Eds. A. Robinson and E. Bernard, *The Sea*, Vol. 15, *Tsunamis* (pp. 201–235), Cambridge, USA: Harvard University Press.
- Mori, N., Takahashi, T., Yasuda, T., & Yanagisawa, H. (2011). Survey of 2011 Tohoku earthquake tsunami inundation and run-up. *Geophysical Research Letters*, 38, L00G14. doi:[10.1029/2011GL049210](https://doi.org/10.1029/2011GL049210).
- Mungov, G., Eblé, M., & Bouchard, R. (2013). DART tsunameter retrospective and real-time data: A reflection on 10 years of processing in support of tsunami research and operations. *Pure and Applied Geophysics*, 170, 1369–1384. doi:[10.1007/s00024-012-0477-5](https://doi.org/10.1007/s00024-012-0477-5).
- Munk, W. H. (1949). Surf beats. *Transactions of the American Geophysical Union*, 30(6), 849–854.
- Parker B. B. (2007). *Tidal Analysis and Prediction*, NOAA Spec. Publ. NOS CO-OPS 3, Maryland: Silver Spring, 378 p.
- Pelinovsky, E. N. (2006). Hydrodynamics of tsunami waves. In: Eds. J. Grue and K. Trulsen, *Waves in Geophysical Fluids. Tsunamis, Rogue Waves, Internal Waves and Internal Tides* (pp. 1–48), Springer, Vienna; doi:[10.1007/978-3-211-69356-8_1](https://doi.org/10.1007/978-3-211-69356-8_1).
- Pugh, D. & Woodworth, P. (2014). *Sea-Level science: Understanding tides, surges, Tsunamis and mean sea-level changes*. UK: Cambridge University Press, 395 p.
- Rabinovich, A. B. (1993). *Long Ocean Gravity Waves: Trapping, Resonance and Leaking*. Gidrometeoizdat, St. Petersburg, 325 p. (in Russian).
- Rabinovich, A. B. (1997). Spectral analysis of tsunami waves: Separation of source and topography effects. *Journal of Geophysical Research*, 102(C6), 12663–12676.
- Rabinovich, A. B. (2009). Seiches and harbour oscillations, in *Handbook of Coastal and Ocean Engineering* (edited by Y.C. Kim), Chapter 9, World Scientific Publ., Singapore, 193–236.
- Rabinovich, A. B., Candella, R. N., & Thomson, R. E. (2013a). The open ocean energy decay of three recent trans-Pacific tsunamis. *Geophysical Research Letters*. doi:[10.1002/grl.50625](https://doi.org/10.1002/grl.50625).
- Rabinovich, A. B., & Eblé, M. C. (2015). Deep ocean measurements of tsunami waves. *Pure and Applied Geophysics*, 172(12), 3281–3312. doi:[10.1007/s00024-015-1058-1](https://doi.org/10.1007/s00024-015-1058-1).
- Rabinovich, A. B. R., & Thomson, R. E. (2011). Energy decay of the 2004 Sumatra tsunami in the world ocean. *Pure and Applied Geophysics*, 168(11), 1919–1950. doi:[10.1007/s00024-01-0279-1](https://doi.org/10.1007/s00024-01-0279-1).
- Rabinovich, A. B., Thomson, R. E., & Fine, I. V. (2013b). The 2010 Chilean tsunami off the west coast of Canada and the northwest coast of the United States. *Pure and Applied Geophysics*, 170(9–10), 1529–1565. doi:[10.1007/s00024-012-0541-1](https://doi.org/10.1007/s00024-012-0541-1).
- Rabinovich, A. B., Thomson, R. E., & Stephenson, F. E. (2006). The Sumatra Tsunami of 26 December 2004 as observed in the North Pacific and North Atlantic Oceans. *Surveys In Geophysics*, 27, 647–677.
- Reymond, D., Hyvernaud, O., & Okal, E. A. (2013). The 2010 and 2011 tsunamis in French Polynesia: Operational aspects and field surveys. *Pure and Applied Geophysics*, 170(6–8), 1169–1187. doi:[10.1007/s00024-012-0485-5](https://doi.org/10.1007/s00024-012-0485-5).
- Saito, T., Ito, Y., Inazu, D., & Hino, R. (2011). Tsunami source of the 2011 Tohoku-Oki earthquake, Japan: Inversion analysis based on dispersive tsunami simulations. *Geophysical Research Letters*, 38, L00G19. doi:[10.1029/2011GL049089](https://doi.org/10.1029/2011GL049089).
- Sanchez, A. J., & Farreras, S. F. (1993). *Catalog of Tsunamis on the Western Coast of Mexico* (p. 79). Boulder, CO: National Geophysical Data Center.
- Satake, K., Rabinovich, A. B., Dominey-Howes, D., & Borrero, J. C. (2013). Introduction to “Historical and Recent Catastrophic Tsunamis in the World: Volume 1. The 2011 Tohoku tsunami”. *Pure and Applied Geophysics*, 170, 955–961. doi:[10.1007/s00024-012-0615-0](https://doi.org/10.1007/s00024-012-0615-0).

- Shevchenko, G., Ivelskaya, T., & Loskutov, A. (2014). Characteristics of the 2011 Great Tohoku tsunami on the Russian Far East coast: Deep-water and coastal observations. *Pure and Applied Geophysics*, *171*(12), 3329–3350. doi:[10.1007/s00024-014-0727-1](https://doi.org/10.1007/s00024-014-0727-1).
- Simons, M., Minson, S. E., Sladen, A., et al. (2011). The 2011 magnitude 9.0 Tohoku-Oki earthquake: mosaicking the megathrust from seconds to centuries. *Science*, *332*(6036), 1421–1425. doi:[10.1126/science.1206731](https://doi.org/10.1126/science.1206731).
- Song, Y. T., Fukumori, I., Shum, C. K., & Yi, Y. (2012). Merging tsunamis of the 2011 Tohoku-Oki earthquake detected over the open ocean. *Geophysical Research Letters*, *39*, L05606. doi:[10.1029/2011GL050767](https://doi.org/10.1029/2011GL050767).
- Tang, L., Titov, V. V., Bernard, E. N., Wei, Y., Chamberlin, C. D., Newman, J., et al. (2012). Direct energy estimation of the 2011 Japan tsunami using deep-ocean pressure measurements. *Journal of Geophysical Research*, *117*, 08008. doi:[10.1029/2011JC007635](https://doi.org/10.1029/2011JC007635).
- Thomson, R. E., & Emery, W. J. (2014). *Data Analysis Methods in Physical Oceanology* (3rd ed., p. 716). New York: Elsevier.
- Thomson, R. E., Spear, D. J., Rabinovich, A. B., & Juhász, T. A. (2013). The 2011 Tohoku tsunami generated major environmental changes in a distal Canadian fjord. *Geophysical Research Letters*. doi:[10.1002/2013GL058137](https://doi.org/10.1002/2013GL058137).
- Titov, V. V. (2009). Tsunami forecasting. In A. Robinson & E. Bernard (Eds.), *The Sea* (Vol. 15, pp. 371–400)., Tsunamis Cambridge, USA: Harvard University Press.
- Titov, V., Song, T., Tang, L., Bernard, E. N., Bar-Severt, Y., & Wei, Y. (2016). Consistent estimates of tsunami energy show promise for improved early warning. *Pure and Applied Geophysics*, *173*, 3863–3880. doi:[10.1007/s00024-016-1312-1](https://doi.org/10.1007/s00024-016-1312-1).
- Van Dorn, W. G. (1984). Some tsunami characteristics deducible from tide records. *Journal of Physical Oceanography*, *14*, 353–363.
- Vich, M., & Monserrat, S. (2009). The source spectrum for the Algerian tsunami of 21 May 2003 estimated from coastal tide gauge data. *Geophysical Research Letters*, *36*, L20610. doi:[10.1029/2009GL039970](https://doi.org/10.1029/2009GL039970).
- Watada, S., Ksumoto, S., & Satake, K. (2014). Traveltime delay and initial phase reversal of distant tsunamis coupled with the self-gravitating elastic Earth. *Journal Geophysical Research Solid Earth*, *119*, 4287–4310. doi:[10.1002/2013JB010841](https://doi.org/10.1002/2013JB010841).
- Webb, S. C., Zhang, X., & Crawford, W. (1991). Infragravity waves in the deep ocean. *Journal of Geophysical Research*, *96*(C2), 141–144.
- Wei, Y., Chamberlin, C., Titov, V. V., Tang, L., & Bernard, E. N. (2013). Modeling of the 2011 Japan tsunami: Lessons for near-field forecast. *Pure and Applied Geophysics*, *170*(6–8), 1309–1331. doi:[10.1007/s00024-012-0519-z](https://doi.org/10.1007/s00024-012-0519-z).
- Wilson, R. I., Admire, A. R., Borrero, J. C., Dengler, L. A., Legg, M. R., Lynett, P., et al. (2013). Observations and impacts from the 2010 Chilean and 2011 Japanese tsunamis in California (USA). *Pure and Applied Geophysics*, *170*, 1127–1147. doi:[10.1007/s00024-012-0527-z](https://doi.org/10.1007/s00024-012-0527-z).
- Xing, X., Kou, Z., Huang, Z., & Lee, J. J. (2013). Frequency domain response at Pacific coast harbors to major tsunamis of 2005–2011. *Pure and Applied Geophysics*, *170*(6–8), 1149–1168. doi:[10.1007/s00024-012-0526-0](https://doi.org/10.1007/s00024-012-0526-0).
- Zaytsev, O., Rabinovich, A. B., & Thomson, R. E. (2016). A comparative analysis of coastal and open-ocean records of the great Chilean tsunamis of 2010, 2014 and 2015 off the coast of Mexico. *Pure and Applied Geophysics*, *173*(12), 4139–4178. doi:[10.1007/s00024-016-1407-8](https://doi.org/10.1007/s00024-016-1407-8).

(Received May 4, 2017, revised June 9, 2017, accepted June 10, 2017, Published online June 28, 2017)